MECC 2024 Final Report for the Build & Test Challenge

A) Development of the 3D Printing Prototype for the Mechanical Part of the Wave Energy Converter

Intro

The “Ocean Wave Energy Converter” is a device that aims to transfer energy from ocean waves to compress and decompress air in an enclosed chamber to act as an air pump to generate work that can be rerouted into a turbine to give it enough rotational inertia to turn.

The principle idea of this prototype is to make a way for waves to collide with the discs that would move the reaction rod up and down which would compress the spring attached to the rod inside the air pump cylinder. This spring would then decompress and push the rod back down in a reciprocating reaction. This document demonstrates how a scaled prototype looks. This test was conducted in the kinesiology swimming pool at CSUSM which has the capability to generate artificial waves. The prototype consists of 4 sets of converters attached to a floating platform that connects to miniature turbines through tubes.

Before we discuss the results of this test let's breakdown each 3D component and the methods used to create them. Each 3D model was first created in Solidworks then imported over to Tinkercad for further changes and easy access.

The two primary printers used were Fusion 3 and Anycubic Kobra Max as well as two creality Ender 3’s to speed up the process.

For this report the phrase watertight and airtight are used interchangeably, some early solidwork files were created in a older computer that can’t be accessed at the moment so not all information is available.

3D component #1 reaction rods

The total height of the rod comes out to about 0.8 meters. However this height is too large for any affordable printers to print this as one piece. So the model had to be split into three separate components, the handle(0.2 m), lower rod (0.3 m), and upper rod (0.3 m). Which are screwed together with small threads. The width of the rods are 13.1 millimeters and are printed with the standard 15% infill.

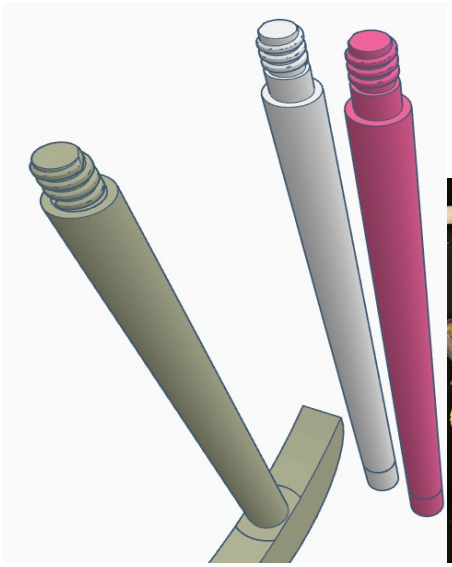

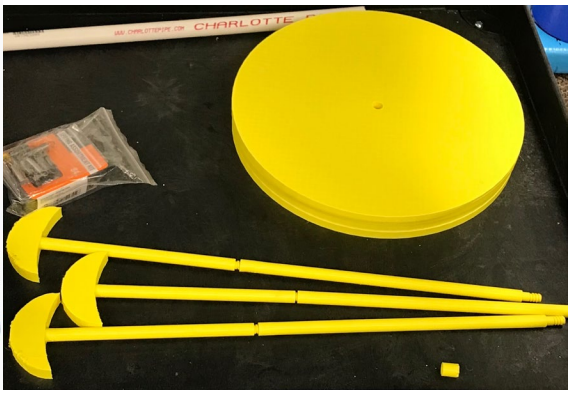

Component #2 Main disc:

The reaction disc is massive at 33 centimeters and 11 millimeters thick, the theory behind this is that its large size will allow it to maximize the amount of energy it could

harness from waves. In order to connect it in between the two rods. It rests on top of the bottom rod and is held together when the top rod is screwed on to it.

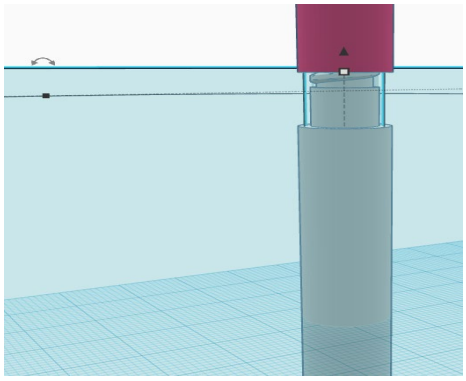

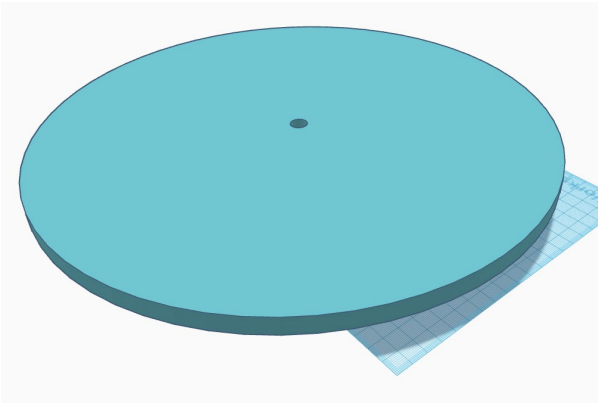

Component #3 Internal disc:

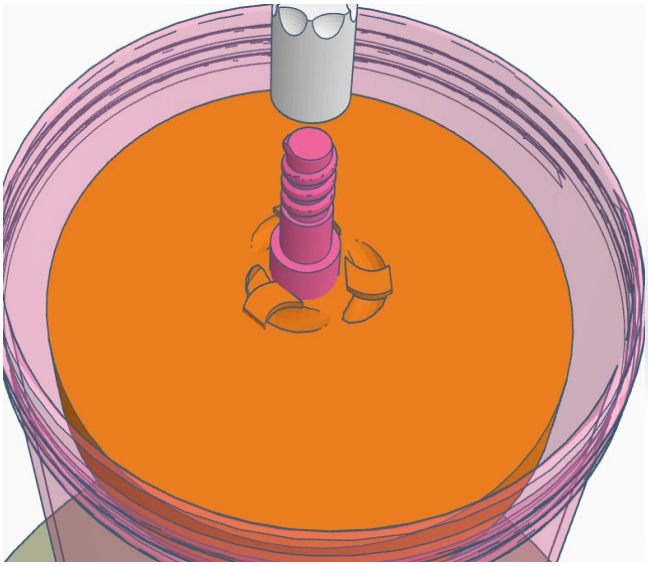

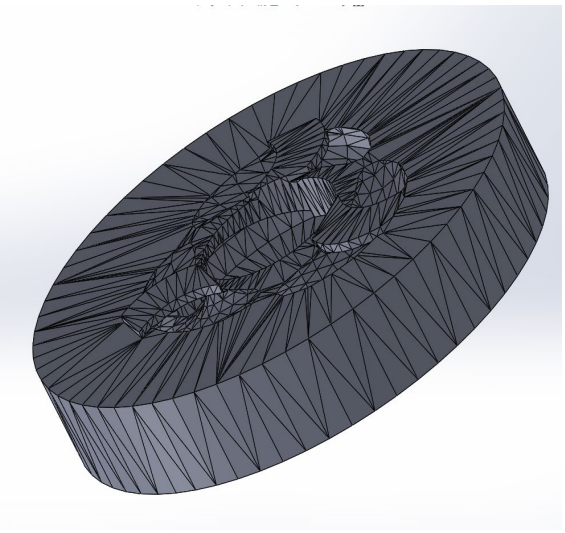

This is the disc that's housed inside of the cylinder. Hooked springs are attached to the three holes in the center which would be attached to the other holes on the cap which have the same mechanism. These hooks are quite strong and don’t break even when

the springs are stretched to the max limit. This disc will be held in place by a small screw that goes in the center which fixes it to the rod. These three holes allow the spring placement to be approached from any angle as well as making room for multiple springs to be used simultaneously for a more robust connection.

Component #4 and #5 Cylinder and Cap Version 1

The initial version of these components were very basic and had to be melted together to be connected.

The first real version aims to emulate a bottle cap with threads that can be opened or closed at any time. Initially the threading on the bottle and cap were both in the same direction. With the thread line in the cap holed into the model. It was essentially one large nut and bolt; the hollowed out threads on the cylinder were made 0.2 mm larger to give room for the threads to screw in without getting stuck. For 3D printing this is essential because all printers have a degree of error in their dimensional accuracy. With enough fine tuning and with a very good printer it’s possible to get the inaccuracy down to >0.1 mm but it’s always a good idea to leave enough room of error for anyone to replicate the print.

While it was functional one glaring issue was still present. The model was not air or watertight, water was leaking out from the point where the cap and cylinder were joined together. The model had to be fully airtight otherwise all air would escape from the chamber and none of it could be harnessed, which would make the whole prototype pointless.

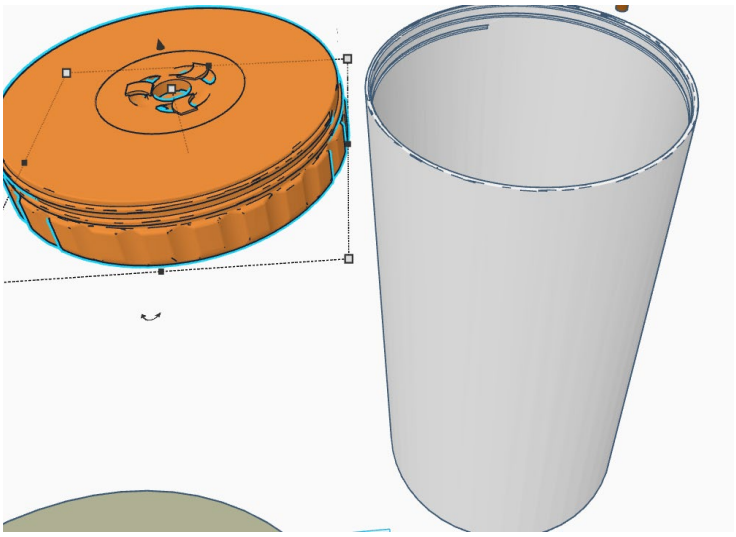

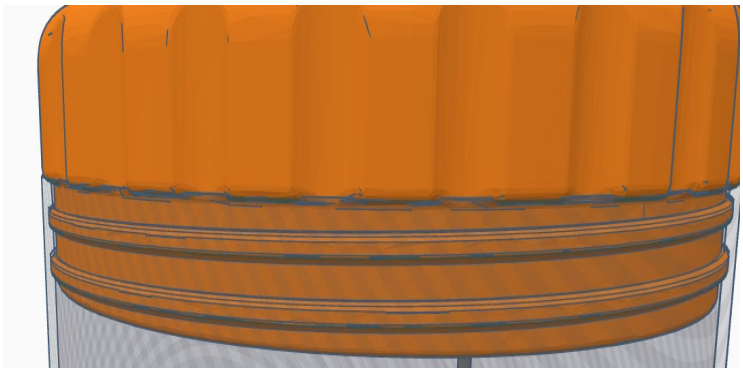

Component #4 and #5 Cylinder and Cap Version 2

For the second version I switched the threads from the inside of the cylinder to the outside of the cylinder. And switched their directions so the cap goes clockwise and the cylinder goes counter clockwise. In order for this to work the sizing of the caps threads have to be small enough to fit in the gaps left behind through each rotation of the cylinders threads.

Also in order to smoothly print these threads it was fileted around the corners and the entry was chamfered into a sharp point. The picture below demonstrates these fillets

and chamfers. Also while presets for threads exist as a feature in solidworks, they are intended for traditional screw shapes. The ones for this project had to be built from the ground up because of the unique shape of these models.

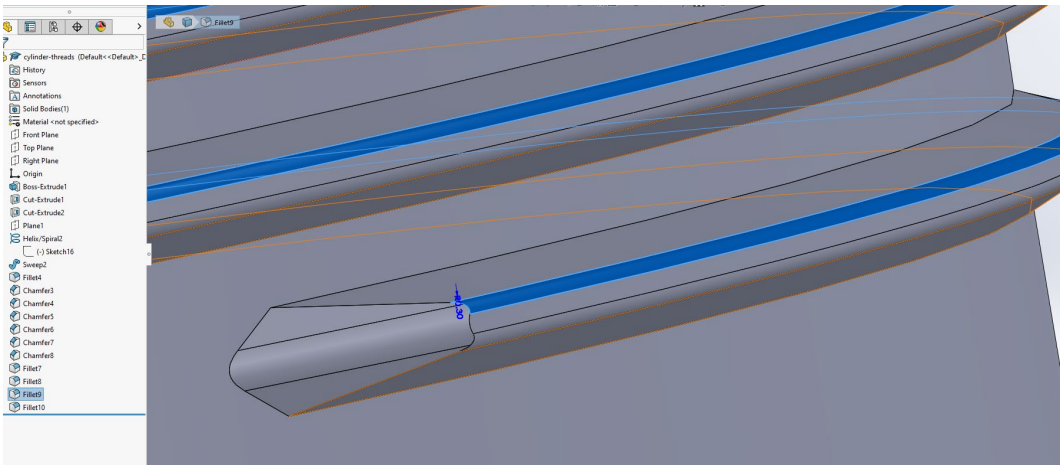

The profile for the threads are described as a congruent trapezoid with a bottom length of 2 mm, to length of 0.75 mm and height of 1.4 mm. The 3D representation of this profile is then swept through a helix until it reaches the top of the cap.
We can then define the revolution, pitch, and direction of a helix and the threads will extrude itself following the path of this helix.

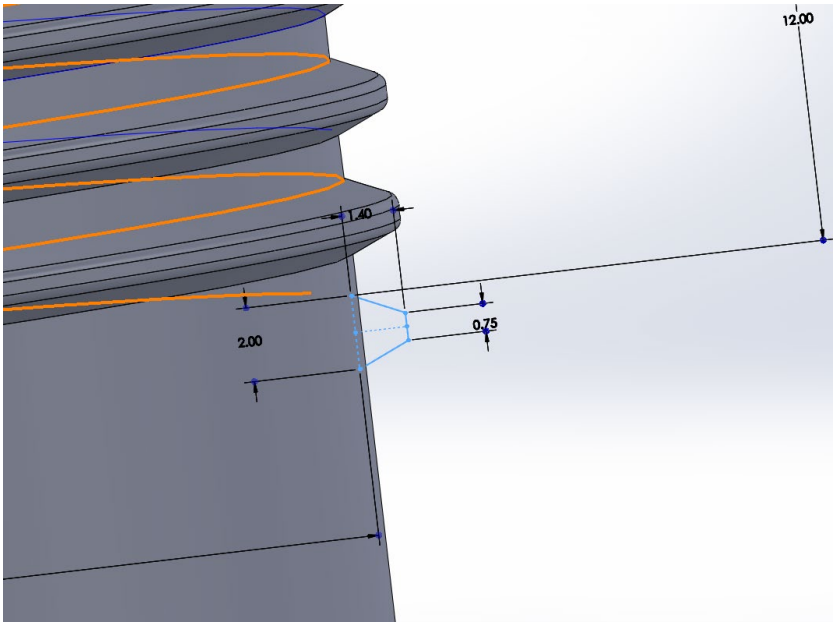

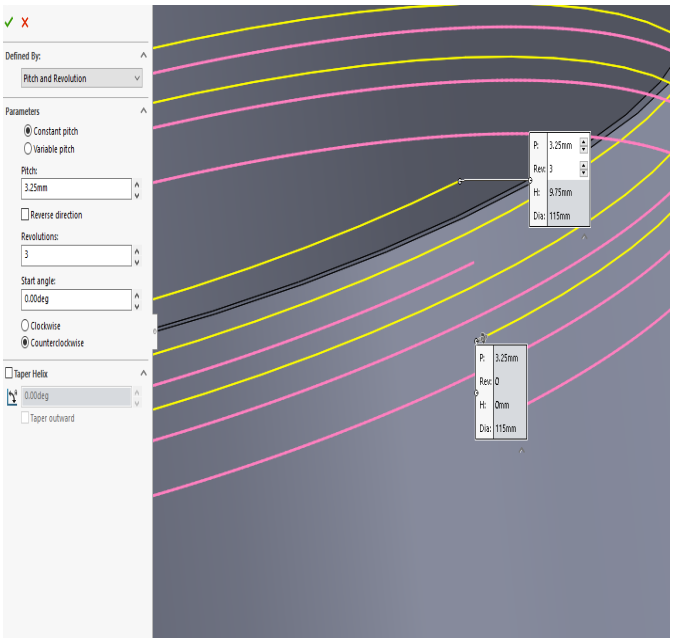

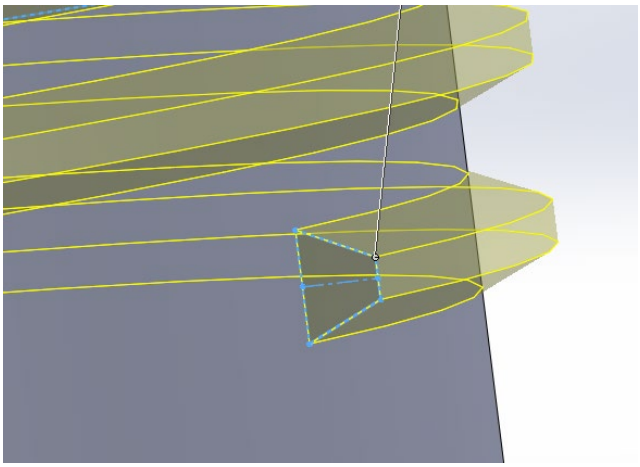

The trapezoidal shaped profile for the cap are set with a bottom length of 1 mm, top length of 0.2 mm, and height of 1 mm. It's less than half the size of the other profile, because the gap between two revolutions is about half the size of one whole thread profile. So these cap threads will twist clockwise into the cylinders threads.

The profile was manually sketched using line and center line tools and placed parallel to the side of the wall.

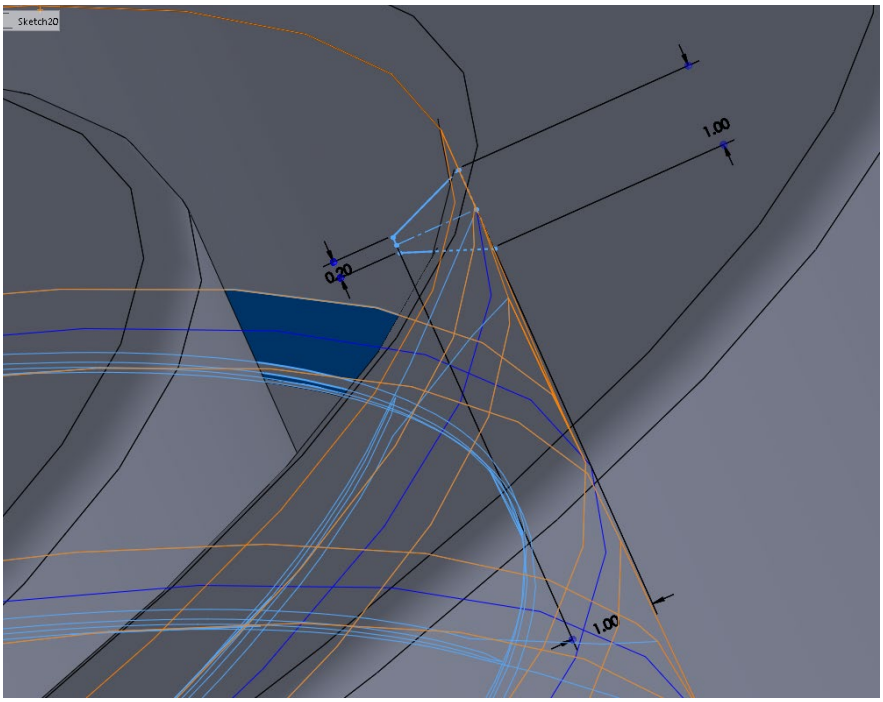

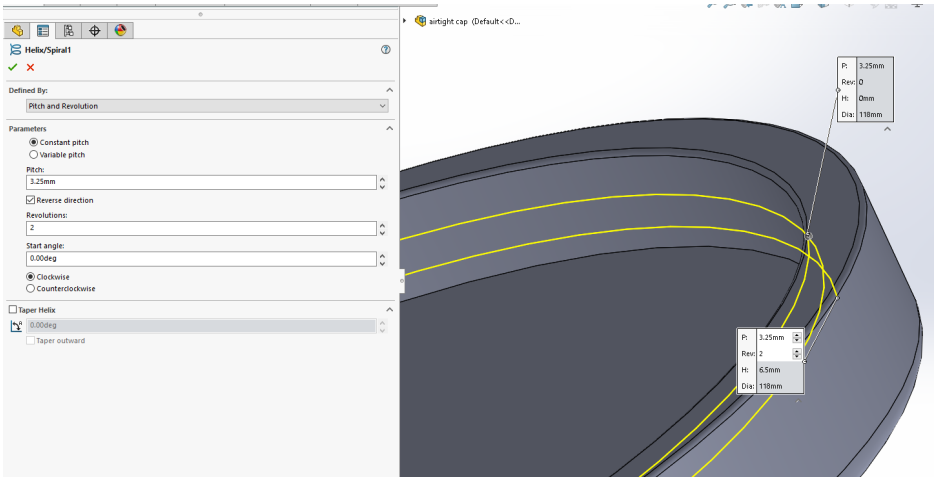

These threads a whole revolution less than the other, this gives ample space to fully close down. In practice, the cap can go about half an extra revolution before it can no longer move at all. It's important that both keep the same constant pitch, which defines the distance before each revolution otherwise they won't be able to fit together. If the cylinder fully tightens then that must mean there is no gap at the top which means no air can escape right? Sadly, when filling the inside with water after a short while there will be leakage. After some investigation it's apparent that its because the top surface of the

printer is not perfectly flat which allows for gaps for fluids to escape. This is a limitation of 3d printing technology and not much can be done to amend it.

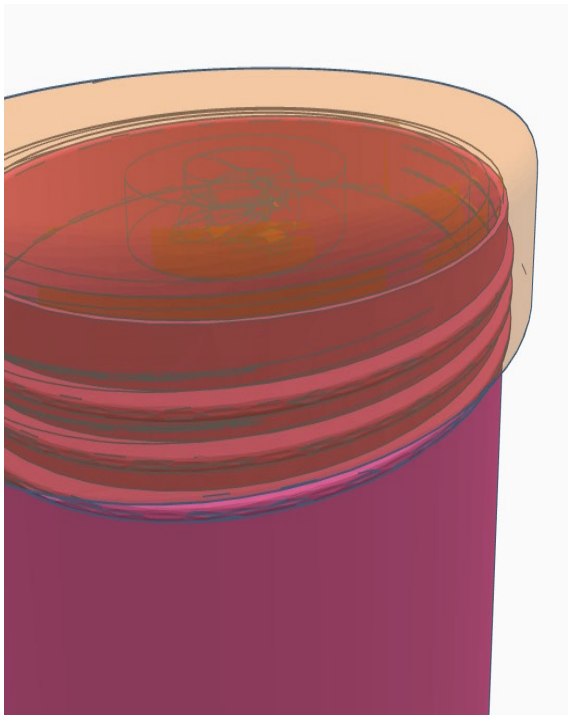

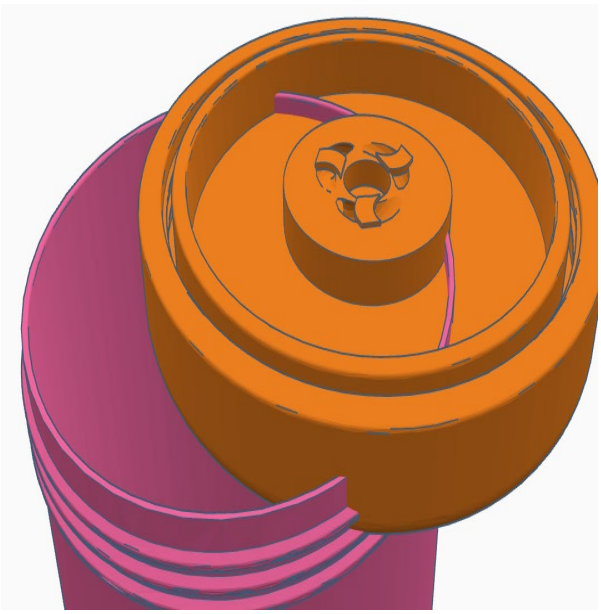

Component #4 and #5 Cylinder and Cap Version 3

The last attempt made was to get rid of the threading and experiment with a new system. This iteration uses a rubber gasket to close the two parts together.

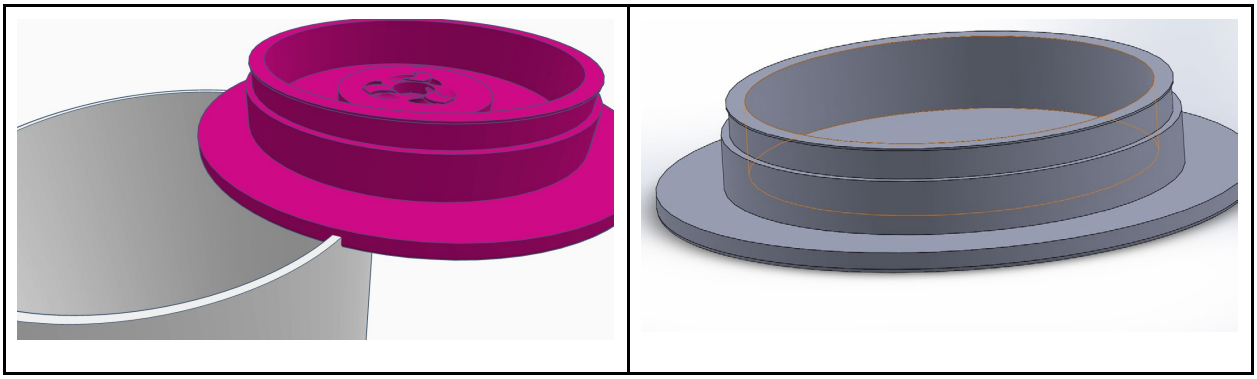

This is a much simpler design concept: simply stretch the gasket into its position and close them together. Would this work? Unfortunately not. It gives the illusion of a watertight fit. But after some time passes, small amounts of water leaks through. So it would seem that the project had hit a road bump, 3D printing is not usually meant to be watertight. It's too difficult to attempt to create a fully watertight model that works right off the print bed. However, with the right post processing it's possible to do so. In hindsight with the right post processing even the first version would have worked.
In this case the product that put this project back on track was "Flex Seal" A liquid rubber sealant product created by the legendary Phil Swift. After twenty four hours the applied flex seal produces a real watertight barrier. The use of this product overcomes the major design challenge that made this project impossible to complete. By covering the entrance point of the cap and cylinder with flex seas so liquid was able to escape

even after being left for a week filled with water.

To view all the models, see this one drive file:Updated models The rest of the prototype pictures and team photos are available here.

Slicer Settings:

The Cura slicer was used for these prints, Slicers work by converting the STL File of a 3D model into G-Code which are instructions that the printer is able to read and follow through in extruding its filament into a specified shape. For most components in this print the standard 0.2 mm layer height and 15% infill was used.
However the cap and cylinder use special settings curated to make the surface watertight and prevent leakage through the material itself.

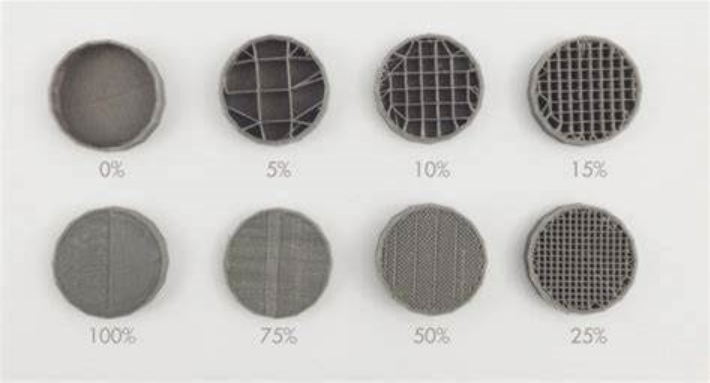

Filament based 3D prints are typically not fully filled in; rather, it has an outer shell and the insides are filled in a pattern that is enough to form the model while using the least amount of material and time. Only the initial bottom and top layers are fully filled in. The bottom layers are fully filled so that the model properly sticks to the bed and has a strong foundation.
It’s common knowledge that bumping up the infill settings produces a more structurally sound model at the cost of time and material. One might think that a 100% infill would fully fill the inside, however in most cases that is incorrect, the infill pattern is still there, it's just really small.
The solution is to actually set the infill to 0%! And from there manually increase the wall and bottom/top layer count to cover the entire model. By doing so we trick the slicer into thinking that it's always printing the bottom layers.

Demonstrating the following with a cap model:

This is what the model looks like under normal settings, the walls are just hollowed in on the inside. Even a small cut or hole on the top layer would reveal the infill patterns.

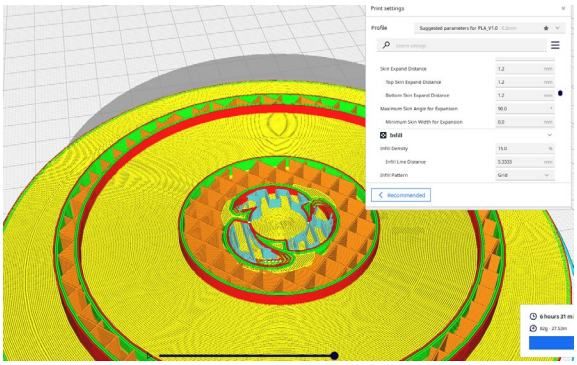

At 0% infill the walls are completely hollow on the inside, printing it as is would be unfeasible and the print would collapse without infill to support it.

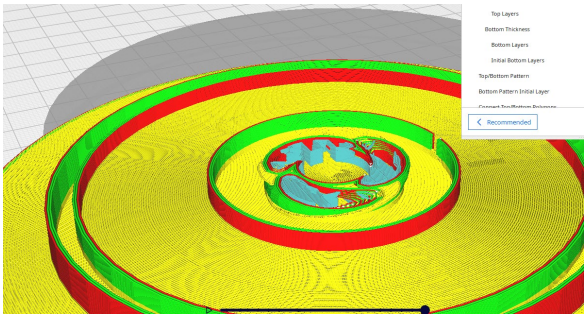

But by changing the wall and bottom/top layer count to its max count we've created a solid piece with no gaps. The walls are denoted by green lines in this preview when comparing it to would normally print the gaps between walls, we see that having more walls make a far more rigid structure.

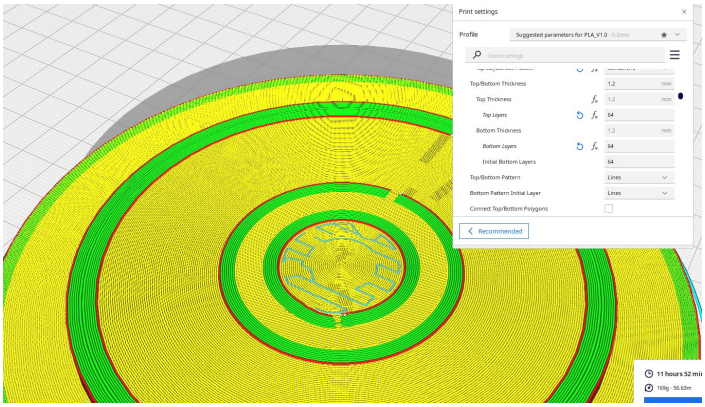

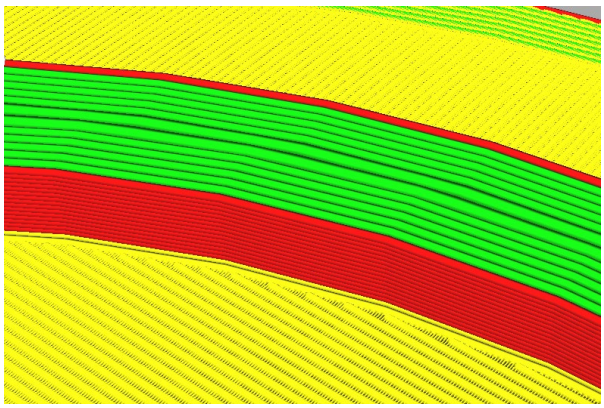

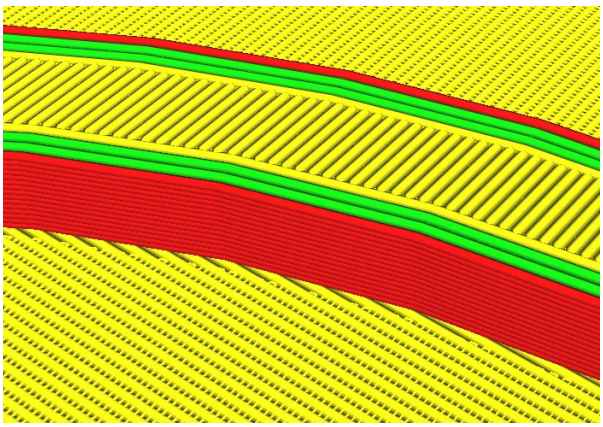

Left: A wall structure with a maxed out wall layer count, each wall is printed at one go of the printer without lifting the nozzle up which creates a more uniform surface with little gaps.
Right: A standard print at 100% infill. The wall count is only a few layers thick and the inside is filled in with infill material, while taking less time overall this method would leave many microscopic holes for air to potentially flow out from.

Other waterproofing methods:

- **Vase mode:**
  When printing a cylindrical circle the nozzle normally draws a single line, lifts up and goes back to a starting point before printing a new layer. This tends to cause seams and gaps each time the nozzle is lifted up and repositioned. One experimental method to remove these seams is to print in Spiralize Outer Contour or “vase mode”. This prints one single wall in a spiral pattern without ever stopping the extrusion, this method is analogous to writing in cursive. While it does produce a wall with no imperfections, unfortunately this mode is only able to produce a shape that's only one wall thick which is too fragile for our goal. Luckily the slicer setting used to define the cap is technically a pseudo or fake “vase mode” because it produces all the effects of what vase mode does

while allowing for more walls. The difference between vase and standard mode is demonstrated in the image below. Enabling the mode will automatically get rid of any roofs and reduce the wall count to one If there were no limitations on wall count vase mode would have been a very useful tool to utilize.

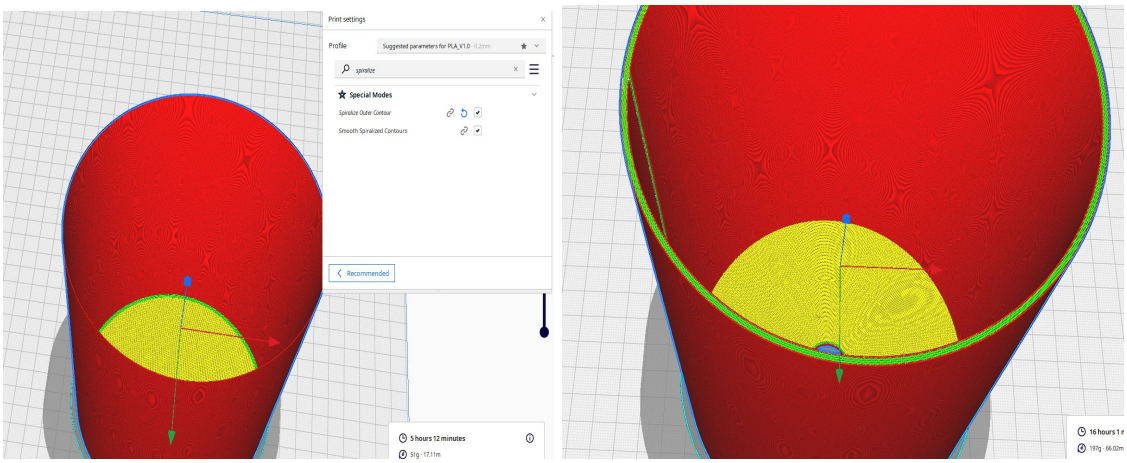

- **<u>Extrusion Width:</u>**

  This setting defines the amount of filament that gets extruded out from the printer. One possible method to create watertight walls is to over extrude your model by setting the flow rate to 120% or more to make the layers overlap with each other and close any gaps. However this is a rather rudimentary method because it tends to cause noticeable blobs and stringing of the material which prevents the threads/gaskets from properly working. Over extrusion can also be achieved by swapping to larger nozzle size for these prints 0.4 mm nozzle was used but a 0.8 mm nozzle would produce similar effects to over extrusion.

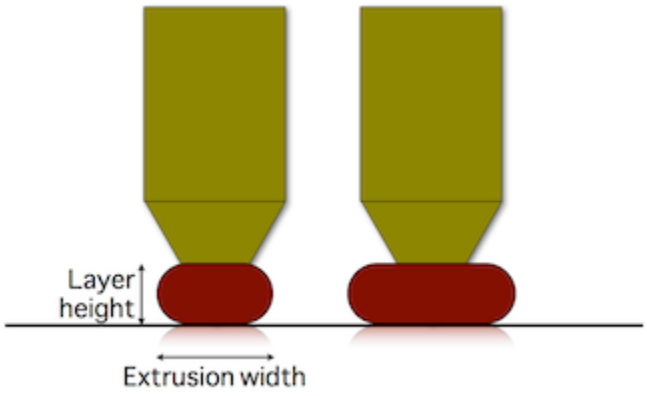

- **Epoxy Resin Coating:**

  This is by far the most effective post processing method at creating watertight prints. An epoxy coating consists of a solution A and solution B that are mixed together in a 2:1 ratio, after a few hours this solution will dry and after twenty four hours it will fully cure. This coating will fill in any gaps and form a clear, glossy surface that is totally air and water tight. This was tested on a print that was only a few walls thick and even after a week there was zero leakage along the walls, showing its effectiveness.

  For the sake of safety this should be done in a well ventilated area while wearing gloves any coating that gets on your skin or eye should be immediately washed away. The coating should also be uniformly brushed across the surface and for maximum effectiveness it should be done on both the inside and outside walls.


The pictures above demonstrate the smooth glossy finish achieved by epoxy coating. It removes visible layer lines and makes a unified surface. It also protects the model from physical damage and reinforces the strength of the spring holders. It's very important to remove any supports before coating otherwise they can’t be removed and not touch or move the print before the coating dries or the layer will be ruined.

Assembly:

The assembly of the prototype was a fairly straightforward process.

Appropriate sized holes were cut into the foam board and was covered with a PVC pipe that was cut and sanded to the correct size. These pipes provide a straight pathway for the rod to move in and out from. The cylinders were then glued on to the platform and a hole was drilled into them to insert tubes that connect to a fan in the center. Careful alignment was required to make sure the hole in the cylinder aligns with the one in the foam board otherside the rods would get stuck. And since this is being glued together with flex seal anything glued together would be close to a permanent connection so there is little room for mistakes. But if the misalignment was small it could be fixed with sandpaper.

Also WD-40 lubricant is used to insure the rods can smoothly move in and out without any friction which would cause significant losses in efficiency. More detailed photos and videos are available in the onedrive marine team file.

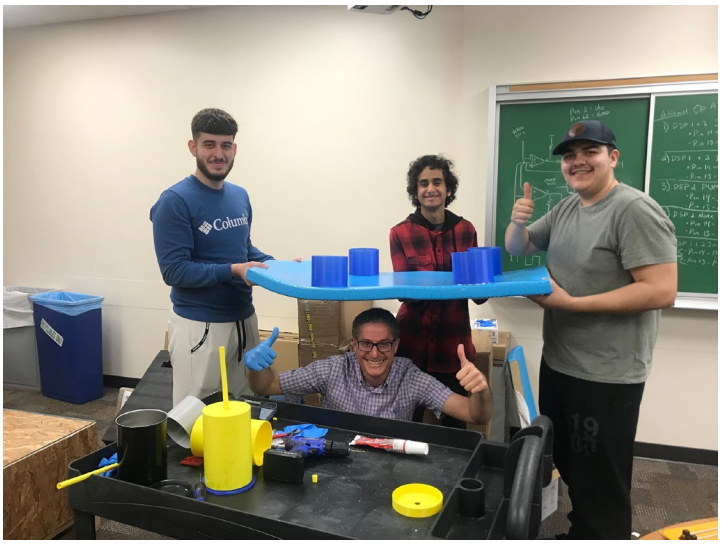

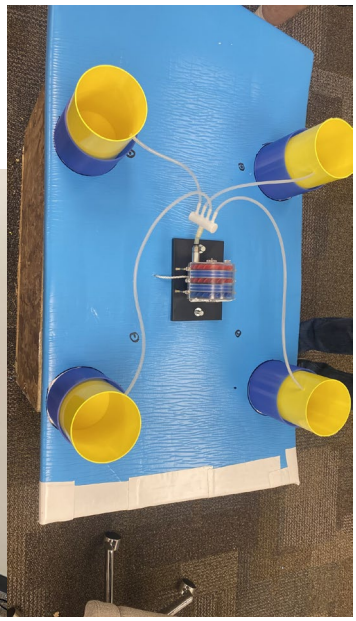

Water Testing:

Initial testing in November showed that the spring does indeed move up and down in a reciprocating reaction. The goal now is to see if this scaled up prototype is able to harness this reaction and turn the small turbines with its compression and decompression of air.

The test was conducted in the kinesiology CSUSM wave pool and at low wave strength the rods were moving up and down as intended, however at strong speeds some things went wrong.

First the top of the cap disconnected from the cylinder. It would seem that the gasket by itself was not enough to hold the assembly in place because as the rod moves up it pushes on the cap and slowly pops it out. The solution to this is to simply revert back to the version that uses threads instead of a gasket. Unfortunately epoxy coating and flex seal was only discovered as an option after we moved on from the version that uses threading. In this rare instance the older version would have worked better than the revised one.

The second issue was that after some time the large disc stopped moving entirely and settled down at the bottom. This was because the inside of the disc started to get filled with water which made it very heavy and removed its buoyancy. This can be avoided by switching to non-water absorbent filament or also coating the discs in epoxy coating but this was neglected until we could see that it did cause problems. Also the discs in general were too large and heavy for this pool.

The third issue was that the joints that connected the rods together were too fragile which resulted in them snapping off at strong wave settings. Looking back up at the mechanism that holds the two rods and the disc together (component #2), it's clear that the thinner midpoint that the disc rests on is very fragile and is the cause for it to snap because the heavy disc rests of the bottom rod puts a lot of weight on it such that it breaks off. The way to fix this is to make the connection point thicker rather than thinner than the entire rod. That way it can handle the pressure, and the way the disc is held together by the rod needs to be changed such that the threads are able to screw into the hole all the way. As it currently stands there is a thin section of the threads that are not able to be inserted

because its whole length is slightly smaller than the thickness of the disc. Also it should be possible to use a feature called selective infill to keep the rest of the rod at low infill but have its screws be printed at 100% infill for maximum strength.

As of now there is no time left to enact these changes and perform another test. But that’s something that can be attempted during summer break. I'm confident that with one more test we will get this prototype to function as intended.

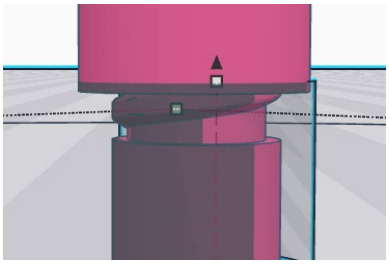

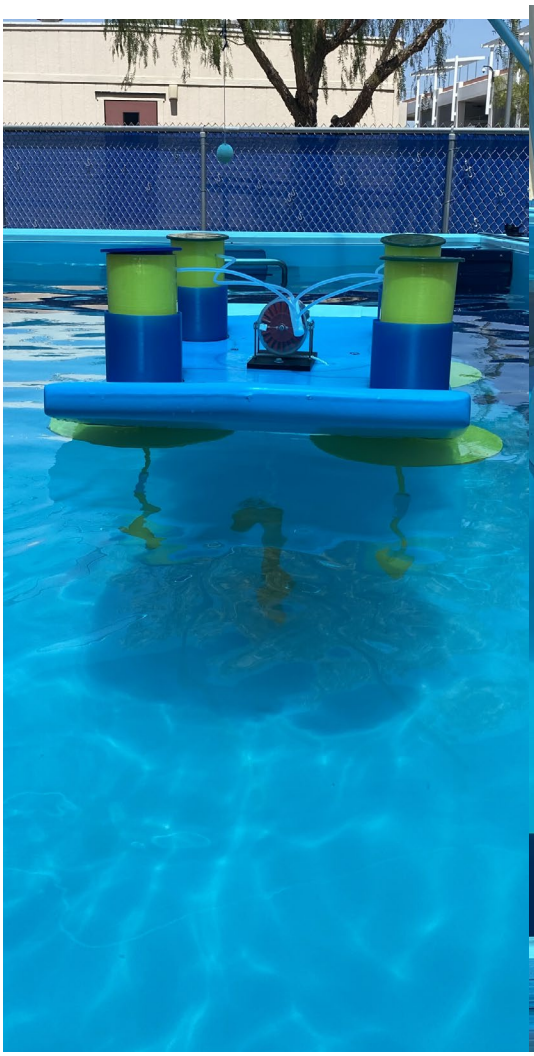

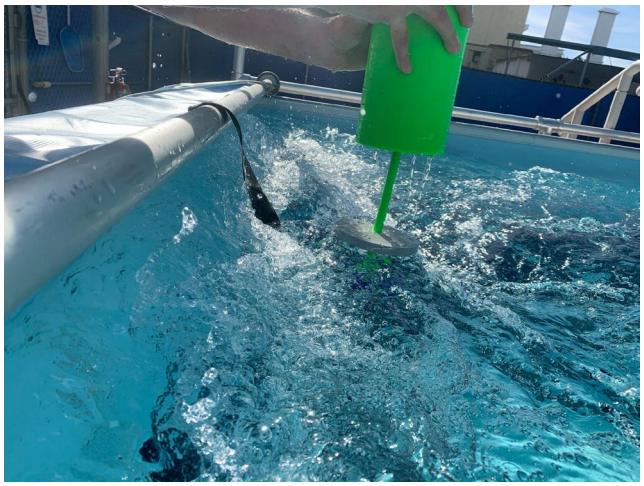

The November prototype was only one small scale set while the final version in April is a more upscaled version closer to our intended vision. While more refinement is

required to verify whether or not this setup has the ability to generate enough energy to turn the turbine, the tests show that this prototype at least works mechanically as a wave-actuated air pump. In that it does have the ability to compress and decompress the springs through up and down movements of the reaction rod/disc.
As it stands the current prototype fails the durability and safety test due to critical failures in its joints and performance fails in strong wave conditions.

Conclusion:

While arguably the simplest part of the MECC challenge, the build and test phase of the project vastly improved our personal 3D printing knowledge and led to the discovery of many helpful tools and tricks that can be used in future projects. The ocean wave energy converter is no longer just a concept but something physical we can see and touch. With only a few more weeks worth of work the 3D printed model can be perfected and next semester we plan on moving on to an actual metallic version.
Harnessing wave energy is within our reach!

B) Hardware Implementation of the Power Take-off System using Modular Multilevel Converter

The modular multilevel converter (MMC) is a voltage source converter which converts DC or AC voltage into DC or AC form of power. This projects focuses on MMC operation in Inverter, DC to AC operating mode. The circuit diagram of this topology in inverter mode is shown in Fig. 1. MMC converter has gained the attention of many industry sectors due to its significant advantages. The MMC has excellent output performance, high modularity, easy bypass of faulty cells in case of a fault, easy scalability of voltage and current, providing high quality of output waveforms. This allows for our converter to avoid placing a physical bulky filter to alleviate harmonics. For the optimal size of our design, the MMC is composed of 6 cells, three cells per each arm. For a sake of simplicity of the converter, the team decided to focus on building a single-phase of our prototype. Inside each cell, there are two metal-oxide-semiconductor field-effect transistors (MOSFET). These MOSFET's act as switches which allow current to pass from Source (S) terminal to Drain (D) when voltage is applied to the Gate (g). They allow our relatively low voltage pulse width modulation signals to turn the switches ON and OFF as indicated in Fig. 2. This occurs in all the six cells with the general rule being that a maximum of three cells can be ON at the same time. The fourth, fifth, sixth cells receive their V+ from the previous cell's V-. When the capacitors charge and discharge, they create an AC sine wave at the load side between the two legs.

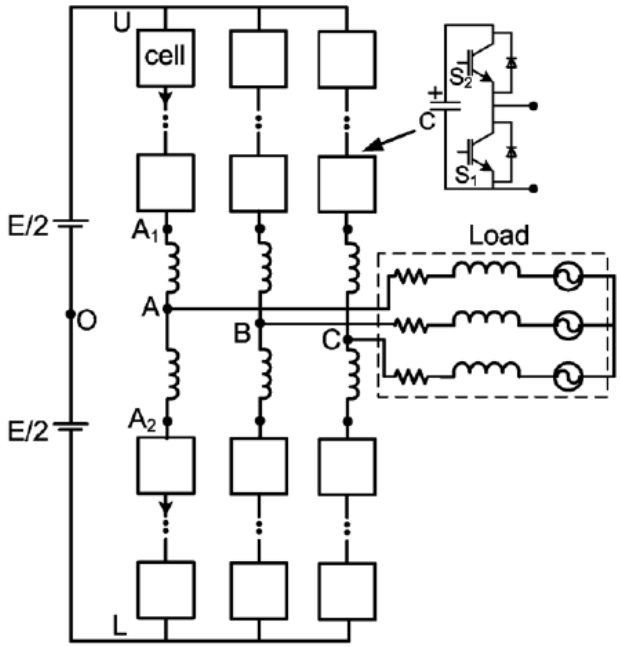

Fig. 1 Circuit diagram of a Modular Multilevel Converter (MMC) in inverter mode (DC-AC)

G1	G2	Capacitor Status
0	0	-----
0	1	DISCHARGING
1	0	CHARGING
1	1	-----

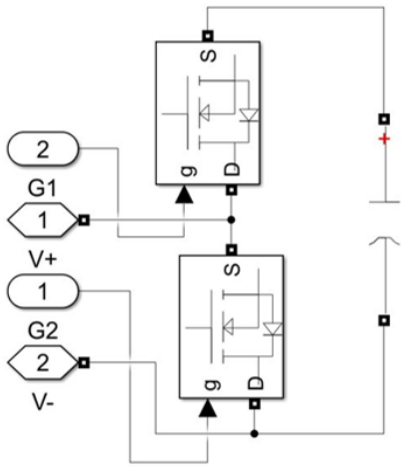

Fig. 2 Configuration of a half-bridge cell of a MMC with switching conditions of the two MOSFETs.

The team developed and assembled the Printed Circuit Boards (CPBs) for the MMC cells and measurement boards. The boards were interfaced with an FPGA board the team programmed. All components in the system were tuned and interfaced together to create a functional system. For the MOSFETs, we utilized 12 IRF540N's from Infineon Technologies. These are rated at 100V, 33A which are suitable for our application.

To ensure operational success intended functionality of this project, the cell level, current and voltage sensors, manual wiring, and the entire 6-cell phase must be made carefully and meticulously. To begin, implementing working cell level design is the first step to completion. Many iterations of a PCB design were created and scrapped due to inaccuracies and better improvements. The schematic in Fig.3 shows the final working prototype that accomplishes all the functions a single cell is required to do.

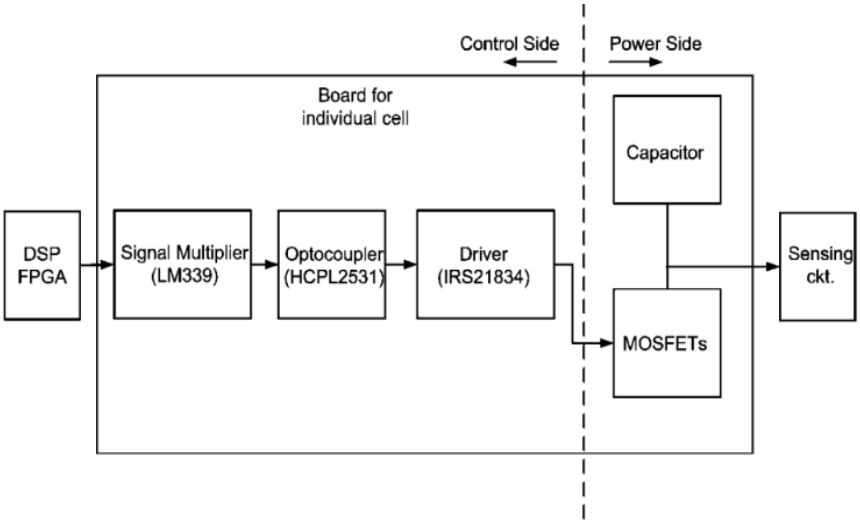

Fig.3 Block diagram of a singular cell showing power and control sections in MMC

As shown in the figure above, the schematic closely resembles the PCB board shown in Fig. 4. Terminals are created near the bottom of the schematic to have a location to insert signals and voltages and receive outputs from the board. The PCB board was wired as closely and similarly to the schematic and block diagram to ensure an easy-to-follow design. Four screw holes were added to the corners to allow for stacking the cells on top of each other. Additional 4 manually drilled holes, depicted as 4 brass rods in the middle of the board in Fig.4, were added to stack a voltage sensor for the cell on top of it. Fig.4 shows the actual PCB board fabricated and assembled.

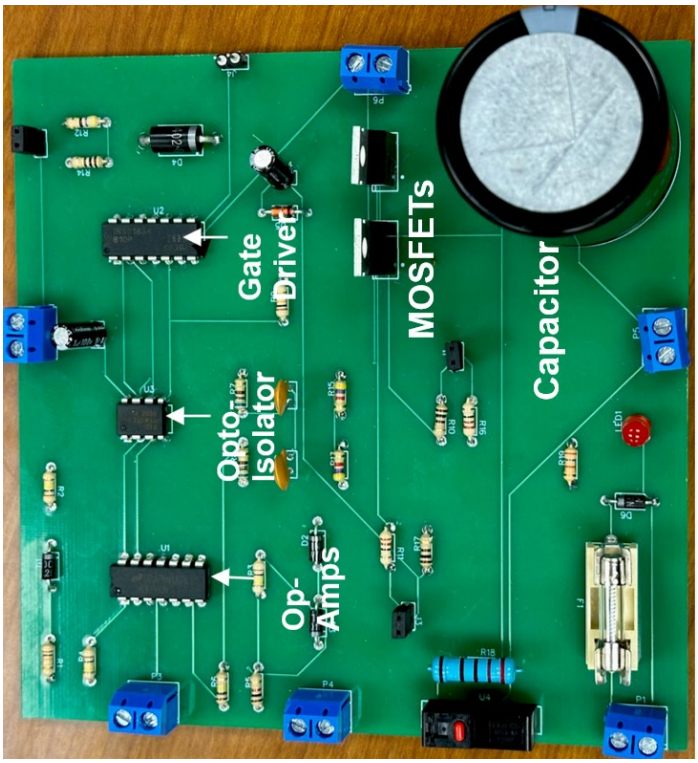

Fig.4 Fully designed with components PCB board

A single cell requires a 15V power supply connected to the terminal “SUPPLY_15V”, a 15V isolated power supply to the terminal “ISOLATED”, and a signal sent from the FPGA into the terminal “IN1.” An additional separate terminal was created for a second PWM signal in case any future projects may require such; but for this project it is shorted. There is one terminal that outputs the voltage of the capacitor (“CAP-S1”) to a voltage sensor and another terminal that is used to cascade each cell (“PWR1”) as shown in the principle operation chapter. Each cell had to be tested individually and measured section by section. In particular, reading outputs and inputs from the LM339 Op-Amp, HCPL2531 Opto-Coupler, and IR21834 Gate Driver. Once the cells were tested and reliably producing the same results without hiccups, the voltage sensors and current sensors had to be tested as well. The voltage and current sensors were previously created, so there was no need to create more. The voltage sensors operate with a 15V supply, the voltage input from the cell capacitor, and a terminal to read the output voltage that has been divided. The voltage sensors that were employed were the LV25-P shown in Fig.5.

Fig.5 LV25-P Voltage Sensor PCB

For this voltage sensor configuration, there is a ratio in which the output reading is calculated. The ratio is calculated and designed to 1:32. For example, if 25V is inputted to the sensor, a reading of .78125V will be read in the output. Each sensor does not satisfy a perfect 1:32 ratio, but the different values can be accounted for inside of the FPGA controller. Each output voltage sensor output will be directly connected to the regular analog inputs (A0-5) of the FPGA board and connected to the FPGA's ground. A reading from a multimeter of the output of a sensor with a 25V input is shown below.

Fig.6 Voltage Sensor reading with 25V input

The current sensors used in this design were the HAIS 100-P current sensors. The sensors themselves do not measure the exact current value, but they can measure its direction. This is enough for our algorithm and the single phase as stated in previous chapters. The Fabricated current sensor on a PCB is shown in Fig.7.

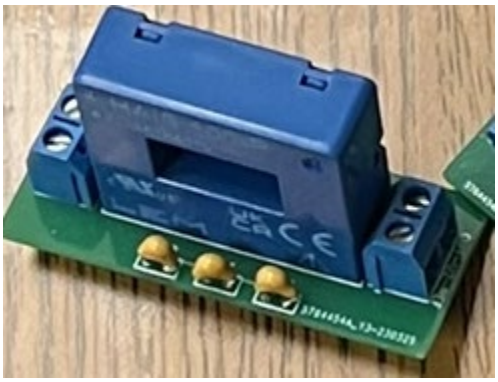

Fig.7 Current sensor PCB

The current sensor is powered via 5V supply and utilizes a reference voltage of 2.5V. A wire is wrapped, with N number of turns, through the center hole which allows the sensor to utilize the Hall effect to measure current direction. When the output voltage is read as higher than the reference voltage, the current direction through the sensor is positive. When the output voltage is read as lower than the reference voltage, the current direction through the sensor is negative. The current sensor output will be connected to the differential input of the FPGA; however, the output voltage must be divided to be within the operational range of 0V to 1V for differential analog inputs. Two small voltage dividers at the end of both current sensors were made to drop the 2.5V output to exactly 0.5V. As shown in Fig.8, a negative current direction is read directly from the output of the sensor.

Fig.8 Current sensor output reading

As seen in Fig.1, in MMC topology each phase has two upper and lower arm inductors are essential for a reliable operation of a MMC converter, such as limiting the arm currents when short circuit happens. The goal range for the inductance was between 1mH and 1.5mH. Through our designs and testing, we were able to theoretically, experimentally, and test the inductors we created. Seen below in Eq.1 is the equation used to calculate the inductance to 1.5mH.

$$L = \frac{\mu_0 * \mu_r * N^2 * A}{l} \qquad \textit{Eq.1}$$

The values in these equations are constants which make this an easier process. $\mu_0 = 1.257 * 10^{-6}$, $\mu_r = 9000$, A = $2.24 * 10^{-3}$, l = 1.85. From here we can bend and simplify the equation to find N, the number of turns of the inductor necessary to achieve the inductance desired.

$$N = \sqrt{\frac{L}{Al}} \qquad \textit{Eq.2}$$

By compressing the previous values, Al becomes a constant value of 13.72 $\frac{\mu H}{N^2}$. From this calculation, it would require roughly 10.46 turns. After this, we utilize the inductive reactance formula $X_L = 2\pi f L$ for our experimentation. We can choose an inductive reactance of any value, using a resistor. By putting this resistor and inductor in series and utilizing a 2-channel oscilloscope and a signal generator, it is possible to measure the inductance of our created inductors. First, the signal generator inputs a signal of any given frequency. The oscilloscope measures the voltage of the resistor on one channel, whilst the other probe measures the voltage of across the inductor as shown in Fig. 9. The goal of this experiment is to increase or decrease the frequency of the signal generator until the voltages across the resistor and inductor match. Utilizing the previous equation, the inductance can be experimentally calculated based on the matching frequency.

$$L = \frac{X_L}{2\pi f} \qquad \textit{Eq.3}$$

By using this experiment, which was difficult due to trouble reading a proper input, we were able to experimentally calculate an inductance of roughly 1.55mH.

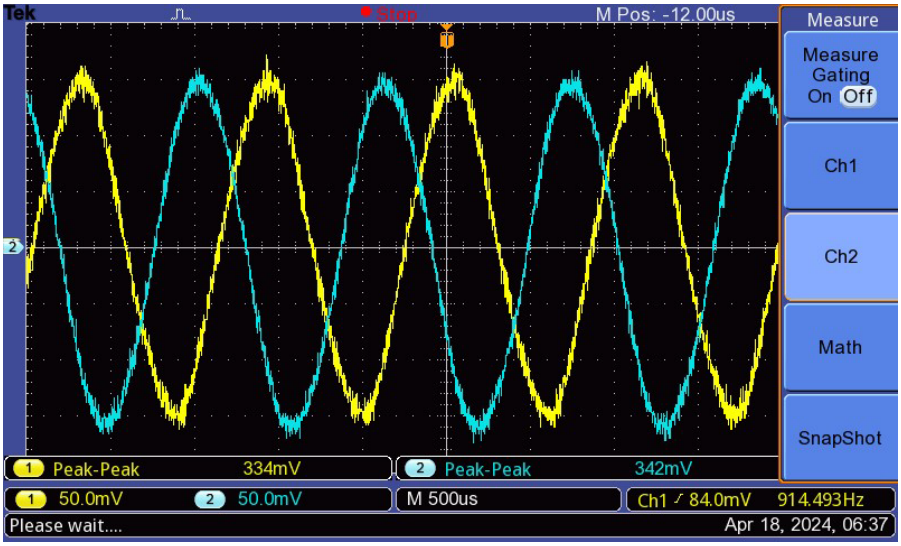

Fig.9 Inductor signal gen vs. voltage across

To ensure these results were correct, an LRC meter was used to confirm our values. For each inductor we received a value of 1.58mH and 1.546mH. With a difference of ~2%, these inductors are well within acceptable parameters to be used as arm inductors.

After ensuring each individual component of the single-phase is working reliably, the full 6-cell MMC prototype was assembled. The entire set-up of the single-phase prototype shown in Fig.10 is built consisting of 3 cells per each upper and lower arms.

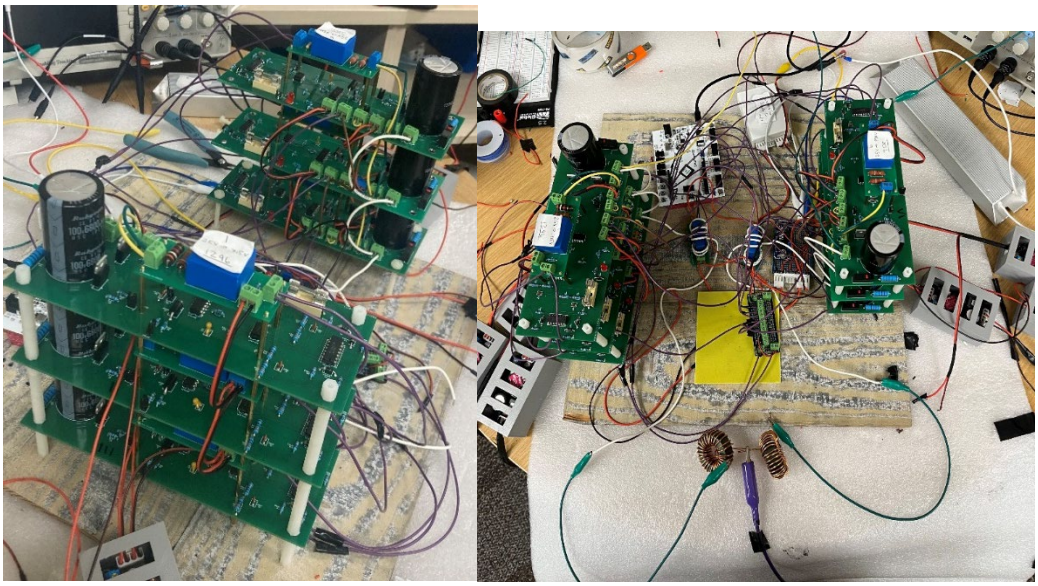

Fig.10 Complete set-up of a single-phase MMC prototype

The prototype is created by stacking cells on top of each other with the voltage sensors on top of the cells they will measure capacitor voltages respectively. Shown in Fig. 10, is the upper and lower arm. A DC bus will be connected to the top of the upper arm and the bottom of the lower arm and will cascade into each other across multiple inductors and output across an AC load. As depicted it is very difficult to maintain concise wiring. One method used to limit the wires is multiple cascades of voltages across each cell. For example, each 15V power supply was cascaded to one another, rather than using three different power supplies.

Experimental Results for the Exemplary AC Loads

The experimental results of this project can be broken down into two sections. The first section is the cell level, and the second section is the full operation of a single-phase prototype.

I. Cell Level Testing

A) LM339 Op-Amp

The main goal of the Op-Amp is to amplify the PWM, boosting the 3.3V peak-to-peak, 2kHz input signal to a 15V peak-to-peak signal. Seen below is the input PWM signal, Fig.11, along with the output of the LM339 Op-Amp, Fig.12.

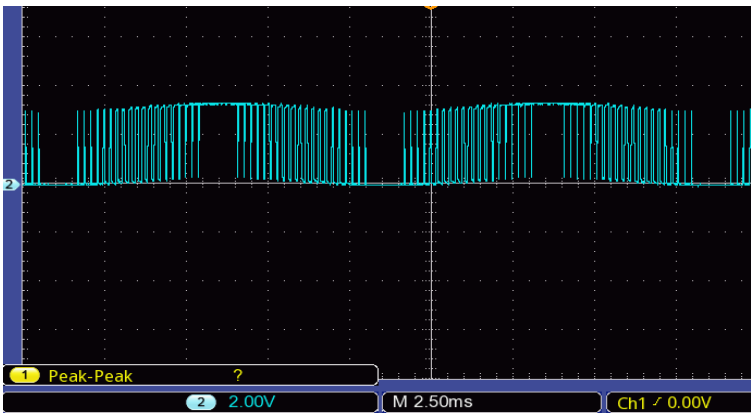

Fig.11 FPGA Input PWM Signal to Cell

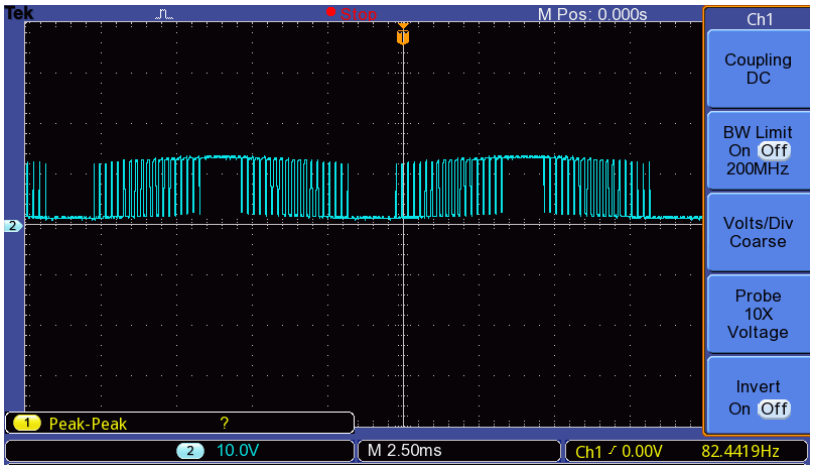

Fig. 12 Output of the LM339 Op-Amp

As is shown in the figures above, the PWM signal is successfully boosted utilizing the LM339 Op-Amp.

B) HCPL2531 Opto-Coupler

Following the cell's structure, the next significant component is the HCPL2531 Opto-Coupler. The goal of this IC, as stated previously, is to smooth and isolate the signal. This is necessary because of the fast-switching frequency inserted into the power section and MOSFETs of the cell. Fig.13 displays the output of the Opto-Coupler, resembling the output of the LM339 closely.

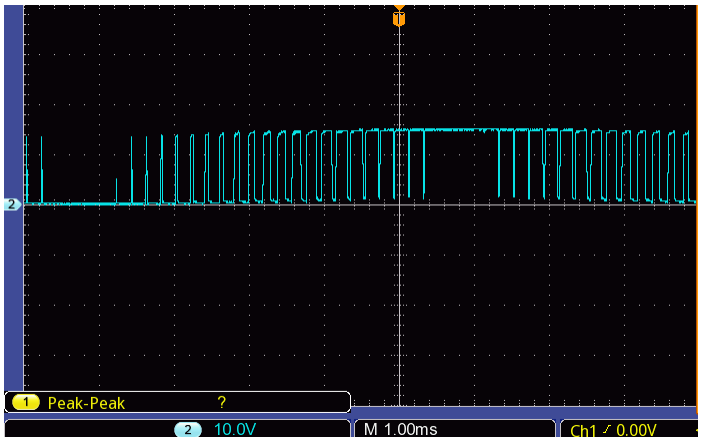

Fig. 13 Output of the HCPL2531 Opto-Coupler

C) IR21834 Gate Driver Board

The following integrated circuit is vital to the task of the cell. As stated previously in the principle operation chapter, the Gate Driver creates two signals, one replicating the original signal and another that is 180° out of phase to control the switching of the MOSFETs. Fig.14 and Fig.15 below display this 180° out of phase operation being conducted.

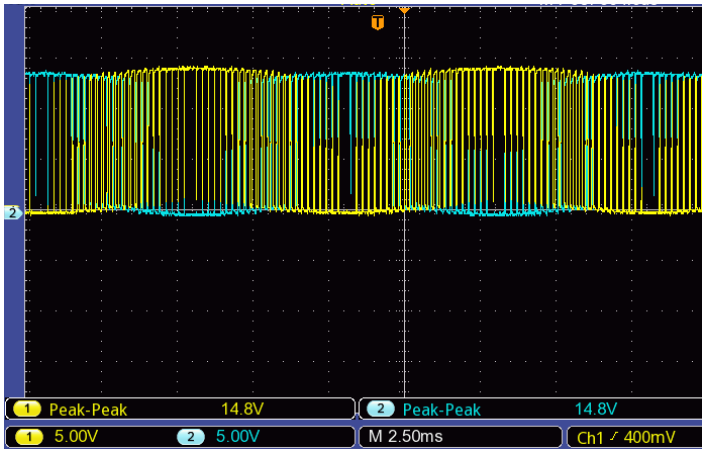

Fig. 14 Output of the IR21834 Gate Driver

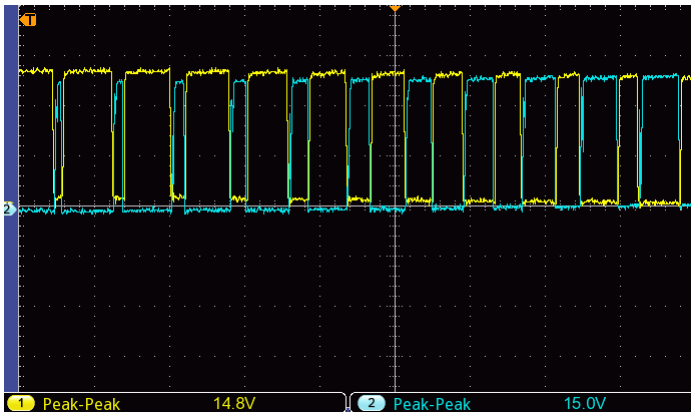

Fig. 15 Zoomed waveform of the IR21834 Gate Driver output

II. Experiments with the complete Single-Phase MMC Set-up

For this experiment in particular, a DC bus was supplied to our system with a voltage of 24V. The system works with the FPGA controller to balance the capacitors around the reference voltage. As previously stated, with 3 cells being in one arm, each capacitor should balance around 8V. Fig.16 shows each capacitor in the system being balanced around this reference voltage. Fig.17 shows the hardware window from the Vivado visualizing all the capacitor voltages; this also shows that the capacitor voltages are on top of each other and the same. In some cases, particularly the bottom arm, there was difficulty in measuring the capacitors. Although correctly reading a balanced voltage around 8V on a multi-meter, when the oscilloscope probes were placed on the output terminal the capacitors would discharge dramatically. Despite this happening, solid outputs were able to be captured across each cell. It can be seen by the ripples in the waves, that this is the FPGA controller balancing the voltage.

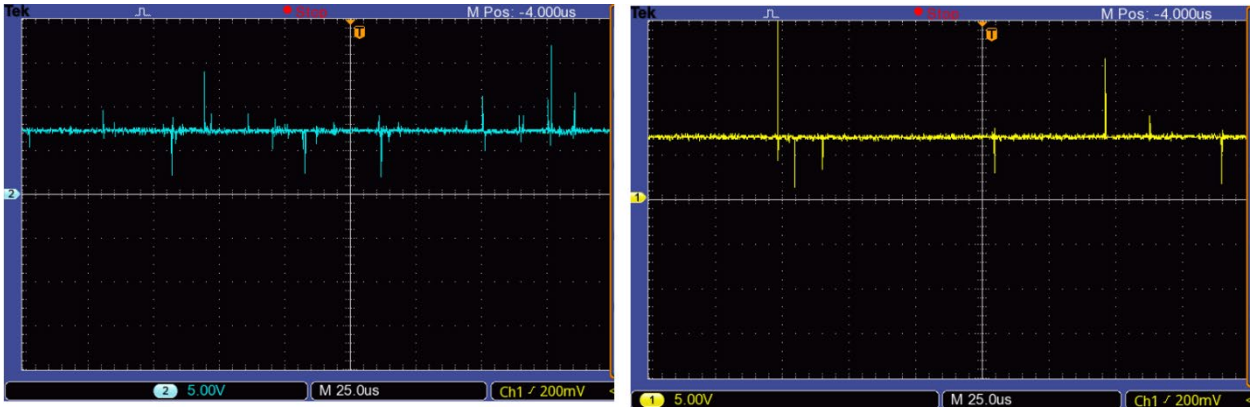

Fig. 16 Capacitor Voltages at Cell 1 of the Upper Arm (Left photo), and Cell 4 of the Lower Arm (Right Photo), capacitors are charged around reference voltage of 8V.

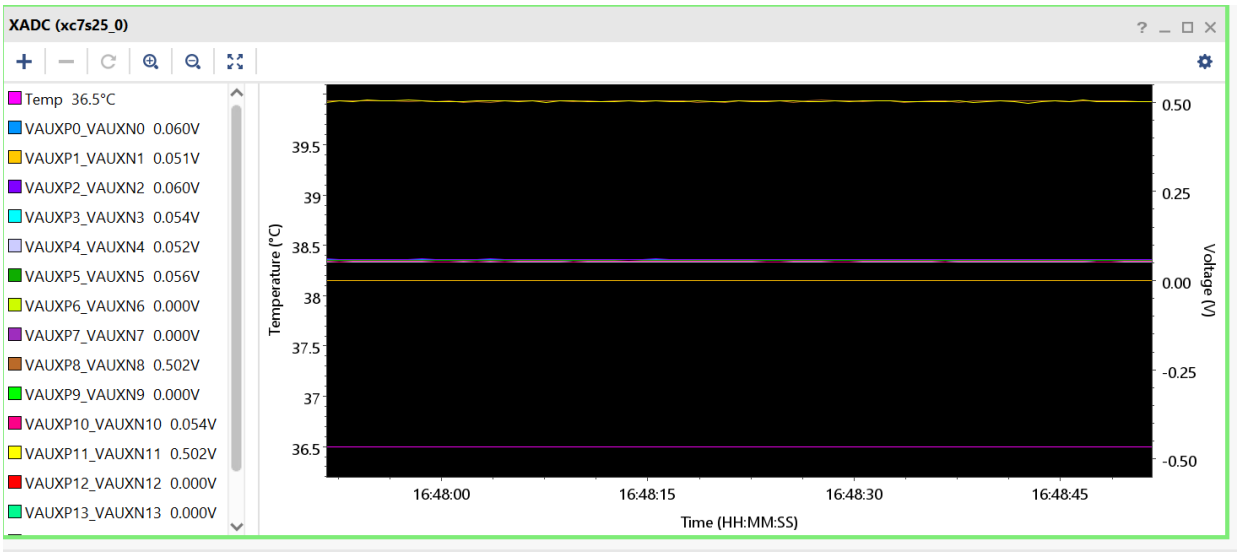

Fig.17 FPGA Hardware Window

Fig.17 shows the bottom multi-colored line along with the readings on the left side of the screen, VauxP0-P5 are balancing accordingly. The top lines are the current sensors being measured checking for direction.

Figs. 18 and 19 show the voltages for the full lower arm and upper arm when an AC motor was used as a load.

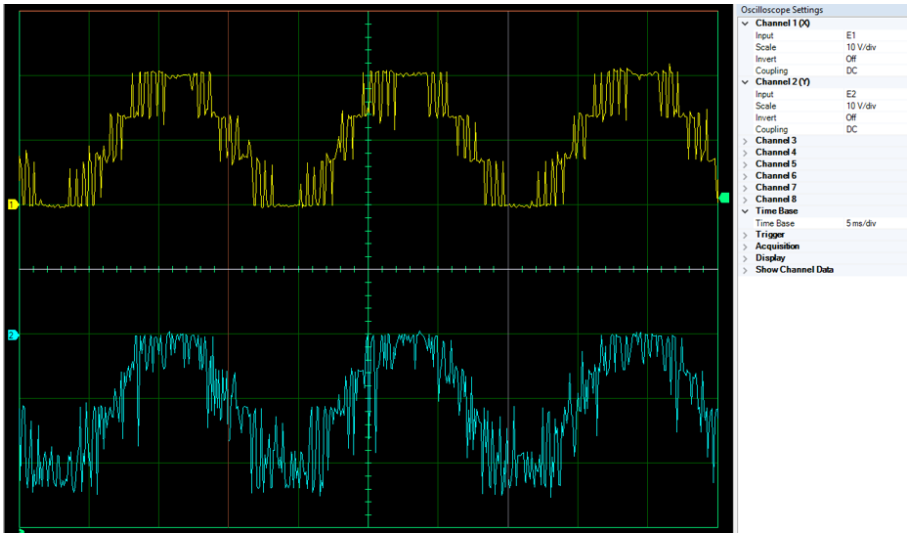

Fig.18 Top Arm (yellow) and Bottom Arm (blue) total voltages

Fig.19 seen below is the combination of the two arm voltages, which is the AC waveform at the inverter output, whilst the bottom wave is the sinewave desired from the MMC output phase current. As it can be seen, a very smooth sinewave is outputted from the MMC prototype without the usage of a filter. This test was conducted on an AC Motor aca load.

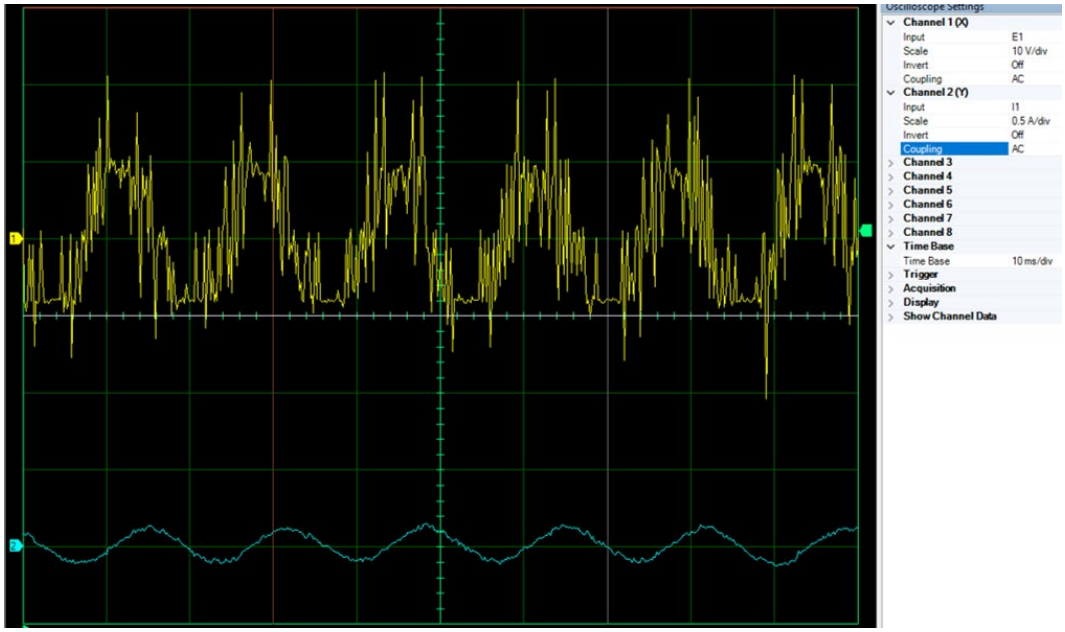

Fig.19 Output Phase Voltage and Current Waveforms for the AC Motor Load

Overall, the results acquired in the prototype testing were reasonable, ultimately deemed successful complying an industry standard such as IEEE-Std. 519 for the power quality and harmonic distortion requirements. There are areas that will be improved upon by using better quality wires to reduce the noise inside of the signals, working in an environment with little electrical disturbance, more efficient inductors, a more powerful FPGA board, or improving the PWM strategy and design. Countless mishaps occurred during this process such as capacitors blowing, ICs malfunctioning, sloppy soldering, incorrect wiring, even an FPGA board getting browned out. Regardless, this prototype has accomplished in creating a working cell level design, a functional capacitor balancing algorithm, as well as an operational full single-phase prototype to generate 60Hz AC power.

Design and Hardware Development of a Modular Power Take-off Topology for Wave Energy Converter Prototype

Prepared for

Marine Energy Collegiate Competition 2024

The National Renewable Energy Laboratory (NREL)

Prepared by:

CSUSM Marine Team

Faculty Advisor:

Dr. Hamed Nademi

College of Science, Technology, Engineering, and Mathematics (CSTEM)
California State University-San Marcos
San Marcos, CA 92096

May, 2024

Marine Team Participants:

(In Alphabetical Order)

—Undergraduate Students—

Alin Hanna
Brent Joel Galindez
Deaven Contreras
Fares Alhabardi
Haley Lorenz
Michael Ross
Miguel Lopez

— Faculty—

Dr. Hamed Nademi

Table of Contents

I. Introduction

Wave energy converters (WECs) are devices which convert the kinetic energy of moving ocean waves into electrical energy. Though the idea has been around for centuries, it has yet to be implemented to address the barriers that have prevented wave energy development in full-scale and will give more insight into the benefits that the technology could bring to communities. Of all the renewable energy sources, ocean wave energy harvesters are often overlooked. One reason for this, is that current technologies are invasive to environments and need to cater to a variety of geographical and financial needs. The ocean contains a vast amount of kinetic energy which should not be overlooked.

The major downside of current renewable energy sources, such as Solar PV and wind energy is their inability to provide consistent electrical output. Wind turbines need a great deal of wind speed to begin creating electricity, which is not guaranteed. Solar is only efficient when the sunlight or irradiance level is adequate, otherwise, a great deal of electrical energy is missed. Consistency is a major benefit of wave energy converters given that they are placed in non-shallow settings [1]-[3]. In some regions, wave energy is large enough to create a considerable portion of the energy mix.

Efficient transformation of wave energy into electricity offers enormous benefits to island and shoreline communities during and after the occurrence of hurricanes, cyclones, and typhoons when grid supply is infeasible and non-grid power sources are necessary. As such, the costs associated with technology for non-grid applications are a point of reference in the proposed study. The empowerment promise for the topic of interest is consistent with the following blue economy markets:

- Isolated Power Systems: Community Microgrids
- Coastal Resiliency and Disaster Recovery
- Ocean Observation and Navigation Systems
- Provide power to Desalination Plants, wastewater treatment systems

A scalable application that offers clear advantages to island communities and nations, for instance by providing a constant supply of drinking water under normal and emergency conditions.

The principal objectives of the team are: 1) Demonstrate a proof-of-concept of a wave energy converter and fabricating of 3D-model prototype, 2) establish connection with regional marine industry for gaining more insights on applicability of the envisioned design, student internships, 3) exploring the advance the power take-off (PTO) architectures to maximize electricity production.

In this context, CSUSM Marine team employs powerful tools to comprehend the working principles of the concept design for developing a small-scale 3D prototype. The intention is to gain skillsets from designing an idea to experimenting with CAD software developer such as SolidWorks. CSUSM Team have tested the 3D prototype using fully automated pool was used to conduct concept design validation in water. The 3D plug and Play mockup model creates and animates the wave energy converter for possible building marketing strategies purposes. Furthermore, it is used to fabricate bench-top models that enable simple research midway experiments to examine motion characteristics, which define the wave energy converter. The experiments using our fully automated pool on campus allowed the team to ascertain the functional behavior of the wave energy converter to refine the design variables, values, and dimensions.

In addition, this report will explore a new implementation of such ocean wave energy harvesters and explore the potential which it has to revolutionize the way we harvest energy. The proposed power take-off topology places a big emphasis on modularity and scalability. In this way, the system can be modified based on the geographical and financial needs. If energy needs to be harvested for a beach side community, then this technology can be implemented on a smaller scale to reduce its impact to the surrounding marine life. If power output is the main priority, then more wave energy converters can be placed in series to harvest more energy. The modularity can be attributed to the modular multilevel converter (MMC) which is a type of converter that has not been implemented in full-scale systems. This technology, however, has been gaining interest recently due to its operational merits.

Being a modular design, single cells can be removed and replaced when necessary. The control system could bypass MMC cells in the case of a faulty situations. Due to the unique design of the MMC cells, challenges were encountered to develop the design.

The report will first provide an outline of the project and describe the theory behind the technology. Next, we will present our MATLAB simulation findings which detail a promising modular multilevel converter system for this wave energy converter. The hardware implementation of this converter will be discussed along with challenges and problems faced along the way. Then, we will present an analysis of our results and explain the social and economic impacts of implementing this converter on a mass-scale. Lastly, we will suggest areas of future exploration and how this technology will be further improved in future endeavors.

A) Technical Approach and Prototype Considerations

The operating schematic and a functional overview of the studied wave energy converter is shown in Figure 1. The figure conceptually presents the main components realizing the device; wave-actuated air pumps supplying an air-jet turbine and enabling a turbine shaft to rotate at nominal speed based on specific project requirement. The converter comprises four independent air pumps that pump air into the turbine at a pressure, velocity and discharge so that the hydrokinetic energy from waves with significant height and period; (with sufficient wave capture width); is transferred onto the mechanical rotation/speed.

With four standalone operating air pumps, in the case of occurring faults in one, or two pumps, the converter operation is expected to sustain, but at a degraded power output capability. In theory, each air pump generates one-fourth of the rated power radiated by the waves within the capture width of the device. A prototype conceptually depicts a 3D prototype. Assuming the prototype is firmly anchored and deploying winch-operated tether allows the device to heave, sway, and surge within the maximum allowable design limits under harsh ocean condition. However, in this simple built prototype, displacement of the device due to unexpectedly high wave surges and hence corresponding preventive measures are beyond the scope of this study. The captured energy in the turbine is harnessed by a permanent-magnet generator coupled to the shaft of turbine to produce intended power at rated speed for the application of interest. The power take-off (PTO) is illustrated in Figure 1. It should be noted that the PTO design is based on modular multilevel power electronics converter in which a single-phase inverter prototype with power level of 0.5-1 kW is constructed. The Inverter output is 110V AC at 60Hz.

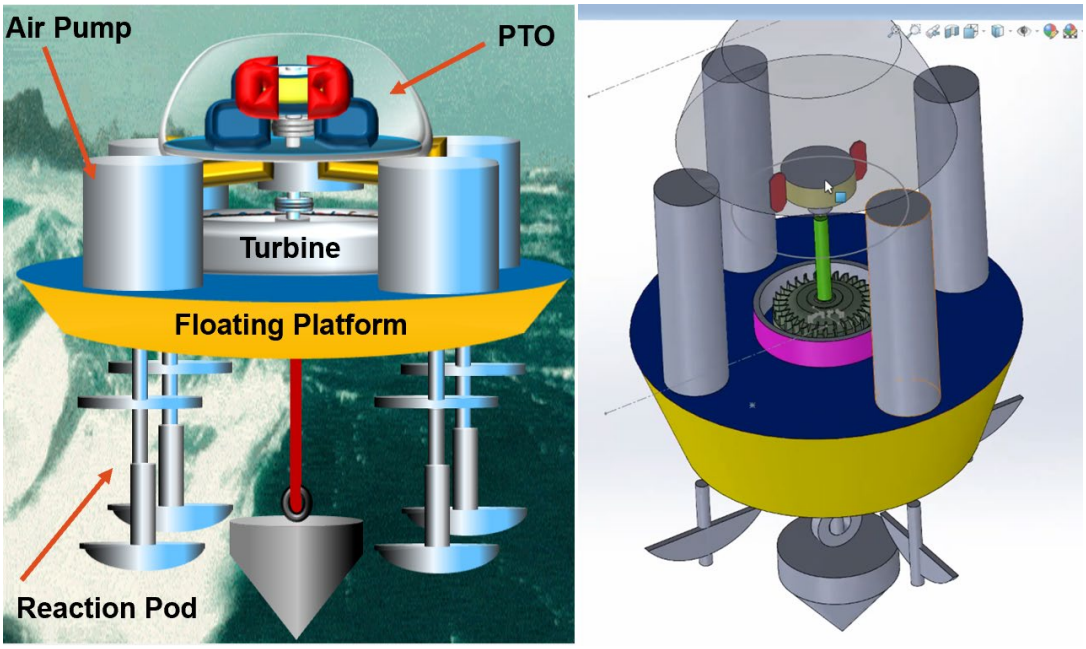

Fig. 1 The operating schematic and main components for the studied wave energy converter and its envisioned 3D prototype developed.

The intention of this project is to bring Marine Energy, particularly wave energy converter knowledge and associated industrial applications to our university and create an opportunity where students from multidisciplinary programs can gain hands-on experience.

There are three major open challenges in the current state-of-the-art WEC technologies [4]-[6]. Firstly, there is a need for a technology that is modular and is scalable such that the WEC can be assembled as a plug-&-play system and deployed rapidly for fast prototyping. Secondly, modularity offers many advantages that, while manufacturing costs can be minimized, the operation and maintenance costs could also be substantially decreased by enabling quick replacement or repair for components affected by failures. Finally, the ease of manufacturing using advanced 3D printing, ease of assembly, transportation, deployment, and the fabrication of spare parts on demand all contribute towards a technology that satisfies the criteria for technology-economic viability.

Advanced/additive manufacturing provides an optimal use of lightweight, high-strength composite materials that considerably improve the buoyancy of the device in response to harsh marine environment.

II. Configuration of the Wave Energy Converter: Wave-to-Wire Structure

As shown in Figure 2, the power electronics conversion units interface the mechanical part with the local loads such as desalination plant and/or utility grid. The power take-off (PTO) mechanism is responsible of transferring the harvested mechanical energy to electrical form.

The topology evaluation and simulation analysis of the entire system along with the obtained results are discussed in consecutive sections.

The proposed all-electric PTO system which is the basis for this conceptual design consists of the key components as:

- Permanent Magnet Synchronous Generator (PMSG)
- AC-DC converter (Rectifier)
- DC-AC converter (Inverter) based on modular multilevel converter (MMC)
- DC-link Capacitor Bus
- Controller

The salient feature of this scheme is that there is no hydraulic or pneumatic stage inside PTO system. The power rating of the generator is fixed at 100 kW. By employing of a fully controlled power electronics converters, complete decoupling of the generator from the utility grid is achieved through DC-link capacitor bank. This implies that the same efficiency in the power extraction from the waves can be guaranteed [7].

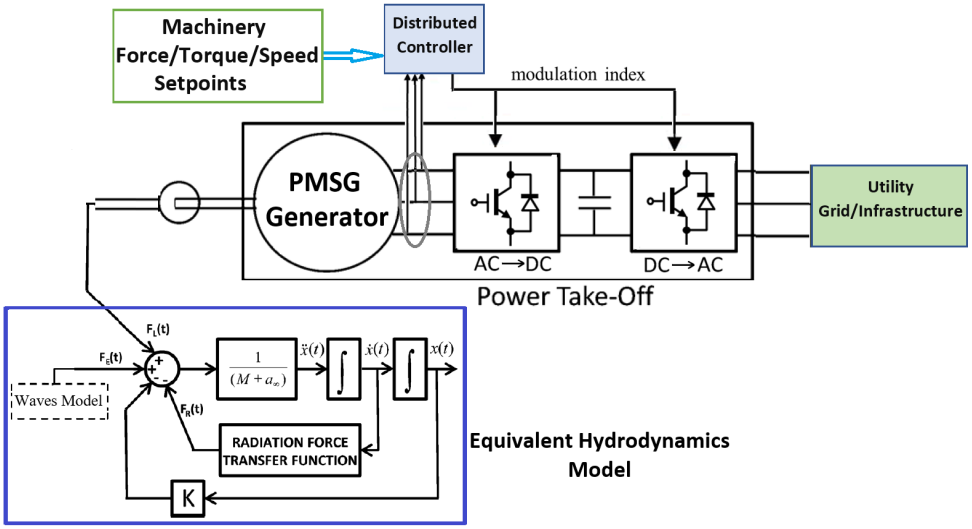

Fig. 2 Configuration of a wave-to-wire model considered in this study which was developed using MATLAB/SIMULINK.

As the design of a rectifier is in the basic sense a very similar to the inverter. For this reason, it was decided within this wave energy converter the new development of the Modular Multilevel Inverter was pursued, therefore a rectifier will not be designed and the SYNDEM Smart Grid Rectifier was used for testing, all the effort as an effect of this were placed on the inverter. However, this inverter can be configured with minor changes as an AC-DC rectifier though.

III. Hardware Development of a Modular Multilevel Inverter

This section first describes the design parameter verification using the Matlab/Simulink model developed to investigate the entire WEC with load. Main simulation results are provided and discussed here. The second part of this section details the hardware design and realization of the single-phase modular multilevel Inverter (MMC) to provide 120VAC, 60Hz power for the load. This includes voltage and current sensors design, power cell construction and control scheme which is implemented in FPGA board.

A) Simulation Analysis using Matlab/Simulink

The team utilized MATLAB Simulink software package to develop the model to demonstrate results and to record datapoints for hardware validation purposes, performance comparison, etc. The simulations assisted with deriving the component parameters, tuning of the PID controller, and to modify the capacitor balancing algorithm. The WEC was modeled to be compatible with the Carlsbad Desalination Plant power requirement [8]. The power rating of the turbine-generator is fixed at 100 kW with nominal speed 950rpm in the simulation analysis. Figure 3 shows the simulation waveform in steady-state wave condition when the turbine shaft speed follows its nominal design value of 950 rpm. There is a delay in acquiring the speed response due mainly to inertia imposed from mechanical part/hydrodynamic model to air-jet turbine that can be observed in Figure 3.

In addition to steady-state operation, the transient response of a simulated system was evaluated when the generator torque reduced by 35% at t=0.5min than the nominal torque value. Figures 4 and 5 show the DC-bus voltage response and generator torque waveform before and after applied transient. As it can be seen from Figure 4, the DC-bus voltage of PTO system illustrates overshoot and undershoot behavior while these variations are returned to the pre-set value after 6 seconds verifying the acceptable performance of the designed control system.

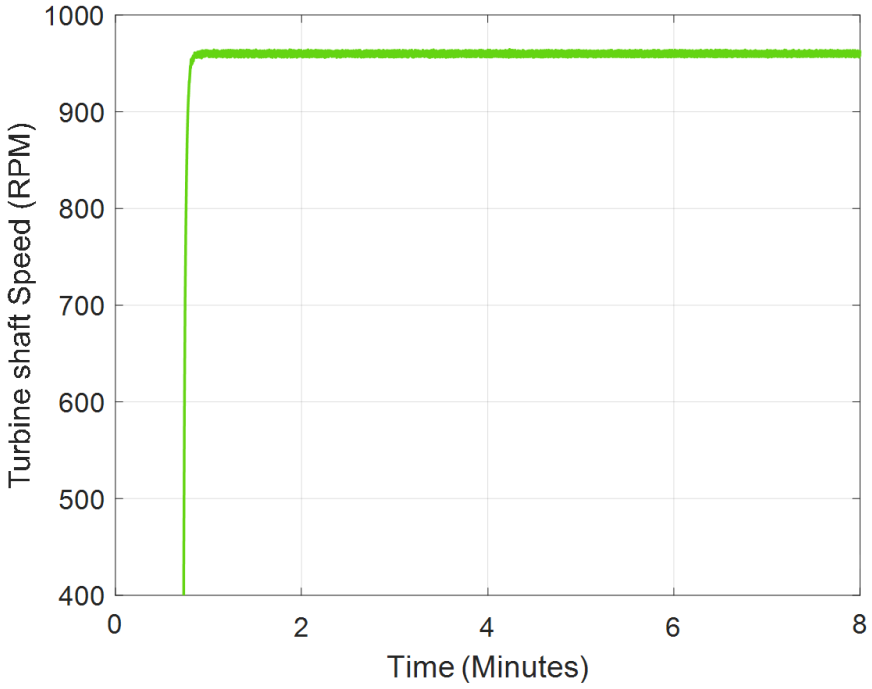

Fig. 3 Simulated response of a turbine shaft speed during steady-state wave condition.

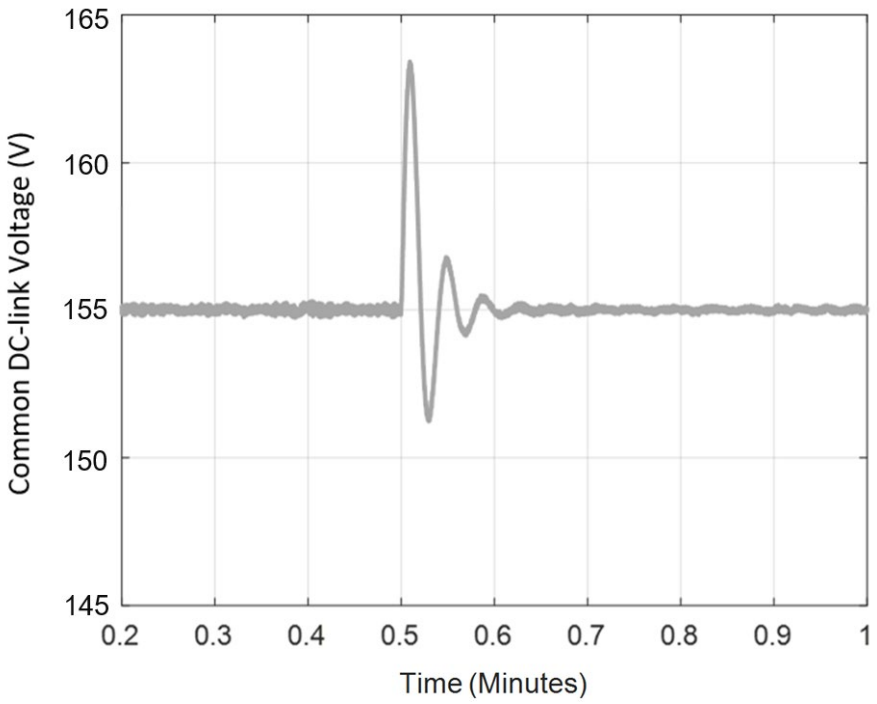

Fig. 4 DC-bus voltage response during transients when generator torque reduced by %35 at t=0.5min.

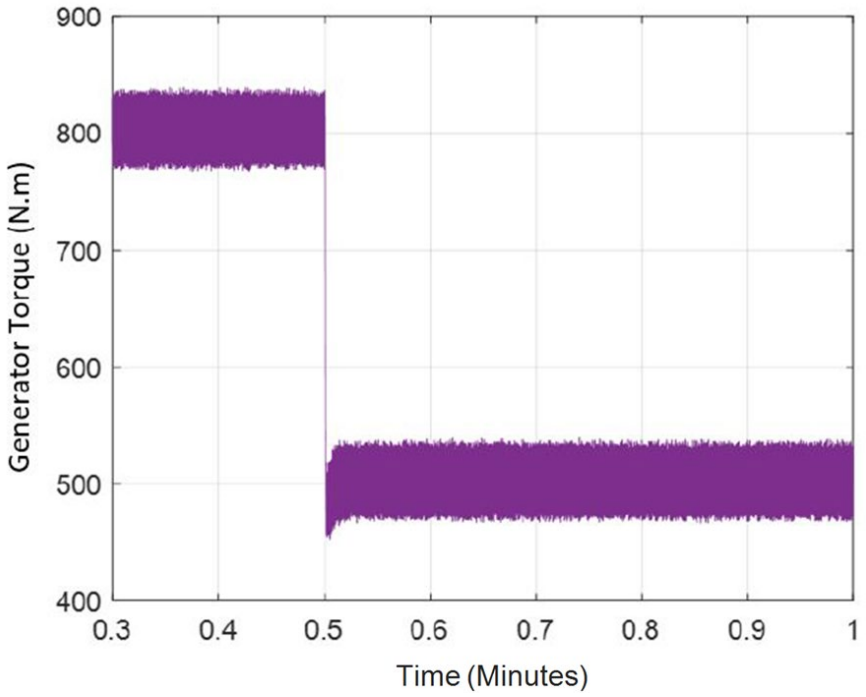

Fig. 5 observed generator torque response when the actual torque setpoint dropped by %35 at t=0.5min.

B) Hardware Implementation of the Power Take-off System using Modular Multilevel Converter

The modular multilevel converter (MMC) is a voltage source converter which converts DC or AC voltage into DC or AC form of power. This project focuses on MMC operation as an Inverter, DC to AC operating mode. The circuit diagram of this topology in inverter mode is shown in Fig. 1. MMC converter has gained the attention of many industry sectors due to its significant advantages. The MMC has excellent output performance, high modularity, easy bypass of faulty cells in case of a fault, easy scalability of voltage and current, providing high quality of output waveforms. This allows for our converter to avoid placing a physical bulky filter to alleviate harmonics. For the optimal size of our design, the MMC is composed of 6 cells, three cells per each arm. For a sake of simplicity of the converter, the team decided to focus on building a single-phase of our prototype. Inside each cell, there are two metal-oxide-semiconductor field-effect transistors (MOSFET). These MOSFET's act as switches which allow current to pass from Source (S) terminal to Drain (D) when voltage is applied to the Gate (g). They allow our relatively low voltage pulse width modulation signals to turn the switches ON

and OFF as indicated in Fig. 2. This occurs in all the six cells with the general rule being that a maximum of three cells can be ON at the same time. The fourth, fifth, sixth cells receive their V+ from the previous cell's V-. When the capacitors charge and discharge, they create an AC sine wave at the load side between the two legs.

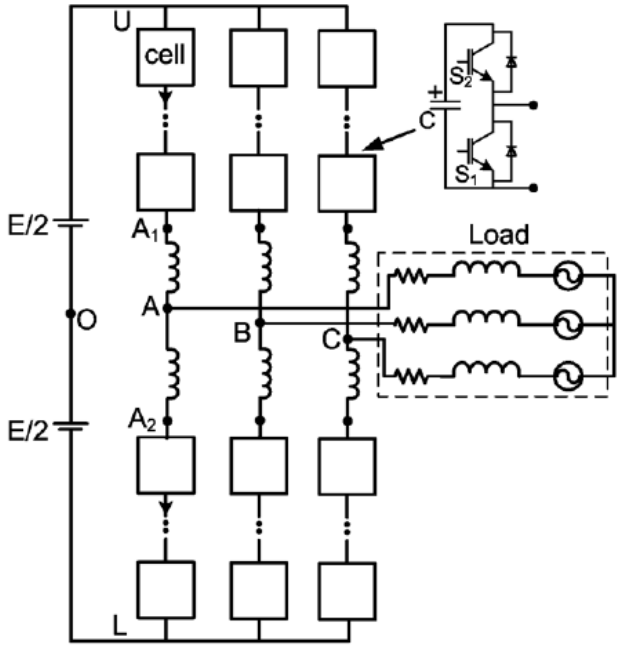

Fig. 1 Circuit diagram of a Modular Multilevel Converter (MMC) in inverter mode (DC-AC)

G1	G2	Capacitor Status
0	0	-----
0	1	DISCHARGING
1	0	CHARGING
1	1	-----

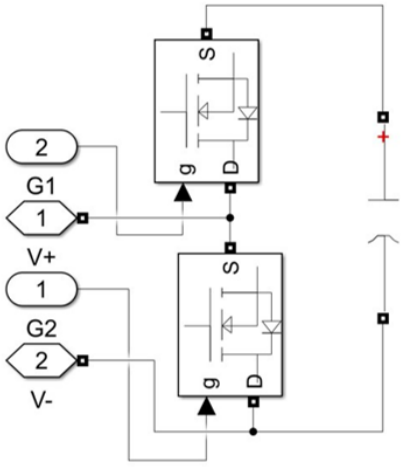

Fig. 2 Configuration of a half-bridge cell of a MMC with switching conditions of the two MOSFETs.

The team developed and assembled the Printed Circuit Boards (CPBs) for the MMC cells and measurement boards. The boards were interfaced with an FPGA board the team programmed. All components in the system were tuned and interfaced together to create a functional system.

For the MOSFETs, we utilized 12 IRF540N's from Infineon Technologies. These are rated at 100V, 33A which are suitable for our application.

To ensure operational success intended functionality of this project, the cell level, current and voltage sensors, manual wiring, and the entire 6-cell phase must be made carefully and meticulously. To begin, implementing working cell level design is the first step to completion. Many iterations of a PCB design were created and scrapped due to inaccuracies and better improvements. The schematic in Fig.3 shows the final working prototype that accomplishes all the functions a single cell is required to do.

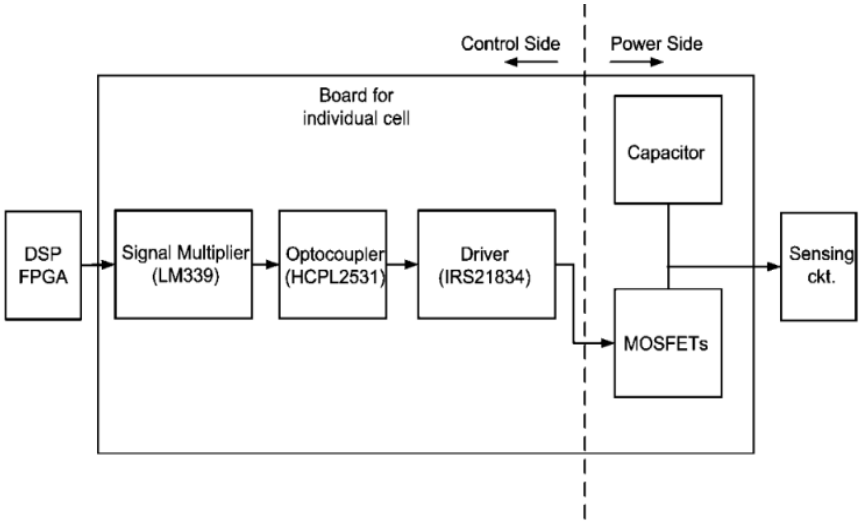

Fig.3 Block diagram of a singular cell showing power and control sections in MMC

As shown in the figure above, the schematic closely resembles the PCB board shown in Fig. 4. Terminals are created near the bottom of the schematic to have a location to insert signals and voltages and receive outputs from the board. The PCB board was wired as closely and similarly to the schematic and block diagram to ensure an easy-to-follow design. Four screw holes were added to the corners to allow for stacking the cells on top of each other. Additional 4 manually drilled holes, depicted as 4 brass rods in the middle of the board in Fig.4, were added to stack a voltage sensor for the cell on top of it. Fig.4 shows the actual PCB board fabricated and assembled.

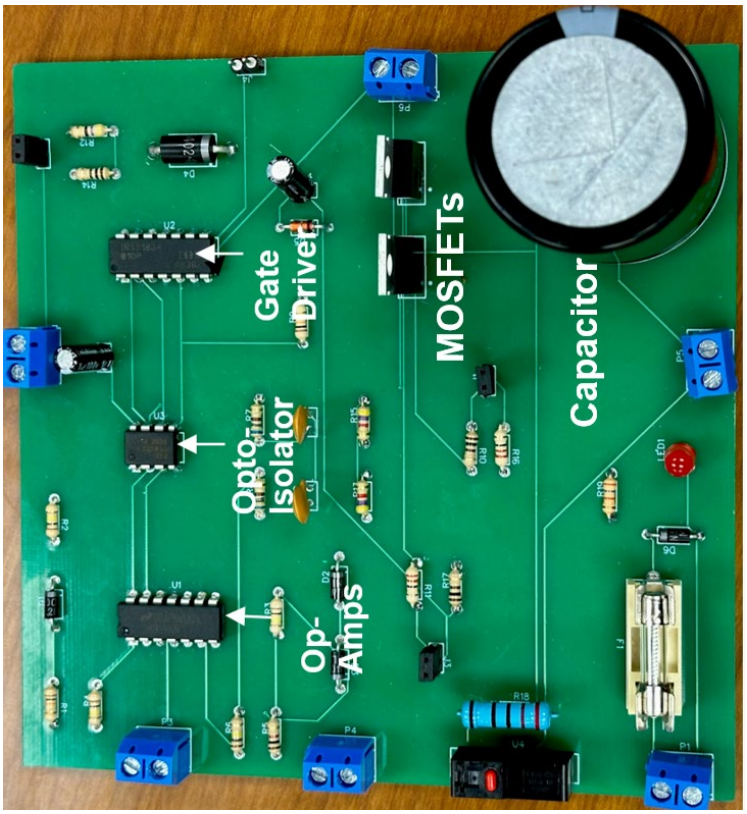

Fig.4 Fully designed and fabricated a cell with components on a PCB board

A single cell requires a 15V power supply connected to the terminal “SUPPLY_15V”, a 15V isolated power supply to the terminal “ISOLATED”, and a signal sent from the FPGA into the terminal “IN1.” An additional separate terminal was created for a second PWM signal in case any future projects may require such; but for this project it is shorted. There is one terminal that outputs the voltage of the capacitor (“CAP-S1”) to a voltage sensor and another terminal that is used to cascade each cell (“PWR1”) as shown in the principle operation chapter. Each cell had to be tested individually and measured section by section. In particular, reading outputs and inputs from the LM339 Op-Amp, HCPL2531 Opto-Coupler, and IR21834 Gate Driver. Once the cells were tested and reliably producing the same results without hiccups, the voltage sensors and current sensors had to be tested as well. The voltage and current sensors were previously created, so there was no need to create more. The voltage sensors operate with a 15V supply, the voltage input from the cell capacitor, and a terminal to read the output voltage that has been divided. The voltage sensors that were employed were the LV25-P shown in Fig.5.

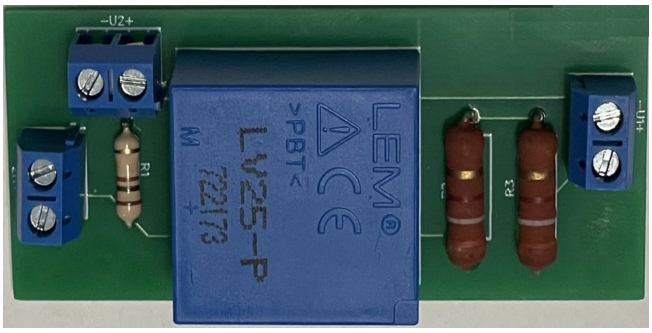

Fig.5 Designed Voltage Sensor fabricated on a PCB

For this voltage sensor configuration, there is a ratio in which the output reading is calculated. The ratio is calculated and designed to 1:32. For example, if 25V is inputted to the sensor, a reading of .78125V will be read in the output. Each sensor does not satisfy a perfect 1:32 ratio, but the different values can be accounted for inside of the FPGA controller. Each output voltage sensor output will be directly connected to the regular analog inputs (A0-5) of the FPGA board and connected to the FPGA's ground. A reading from a multimeter of the output of a sensor with a 25V input is shown below.

Fig.6 Voltage Sensor reading with 25V input

The current sensors used in this design were the HAIS 100-P current sensors. The sensors themselves do not measure the exact current value, but they can measure its direction. This is enough for our algorithm and the single phase as stated in previous chapters. The Fabricated current sensor on a PCB is shown in Fig.7.

Fig.7 Designed Current Sensor fabricated on a PCB

The current sensor is powered via 5V supply and utilizes a reference voltage of 2.5V. A wire is wrapped, with N number of turns, through the center hole which allows the sensor to utilize the Hall effect to measure current direction. When the output voltage is read as higher than the reference voltage, the current direction through the sensor is positive. When the output voltage is read as lower than the reference voltage, the current direction through the sensor is negative. The current sensor output will be connected to the differential input of the FPGA; however, the output voltage must be divided to be within the operational range of 0V to 1V for differential analog inputs. Two small voltage dividers at the end of both current sensors were made to drop the 2.5V output to exactly 0.5V. As shown in Fig.8, a negative current direction is read directly from the output of the sensor.

Fig.8 Current sensor output reading

As seen in Fig.1, in MMC topology each phase has two upper and lower arm inductors are essential for a reliable operation of a MMC converter, such as limiting the arm currents when short circuit happens. The goal range for the inductance was between 1mH and 1.5mH. Through our designs and testing, we were able to theoretically, experimentally, and test the inductors we created. Seen below in Eq.1 is the equation used to calculate the inductance to 1.5mH.

$$L = \frac{\mu_0 * \mu_r * N^2 * A}{l} \qquad \textit{Eq.1}$$

The values in these equations are constants which make this an easier process. $\mu_0 = 1.257 * 10^{-6}$, $\mu_r = 9000$, A = $2.24 * 10^{-3}$, l = 1.85. From here we can bend and simplify the equation to find N, the number of turns of the inductor necessary to achieve the inductance desired.

$$N = \sqrt{\frac{L}{Al}} \qquad \textit{Eq.2}$$

By compressing the previous values, Al becomes a constant value of 13.72 $\frac{\mu H}{N^2}$. From this calculation, it would require roughly 10.46 turns. After this, we utilize the inductive reactance formula $X_L = 2\pi f L$ for our experimentation. We can choose an inductive reactance of any value, using a resistor. By putting this resistor and inductor in series and utilizing a 2-channel oscilloscope and a signal generator, it is possible to measure the inductance of our created inductors. First, the signal generator inputs a signal of any given frequency. The oscilloscope measures the voltage of the resistor on one channel, whilst the other probe measures the voltage of across the inductor as shown in Fig. 9. The goal of this experiment is to increase or decrease the frequency of the signal generator until the voltages across the resistor and inductor match. Utilizing the previous equation, the inductance can be experimentally calculated based on the matching frequency.

$$L = \frac{X_L}{2\pi f} \qquad \textit{Eq.3}$$

By using this experiment, which was difficult due to trouble reading a proper input, we were able to experimentally calculate an inductance of roughly 1.55mH.

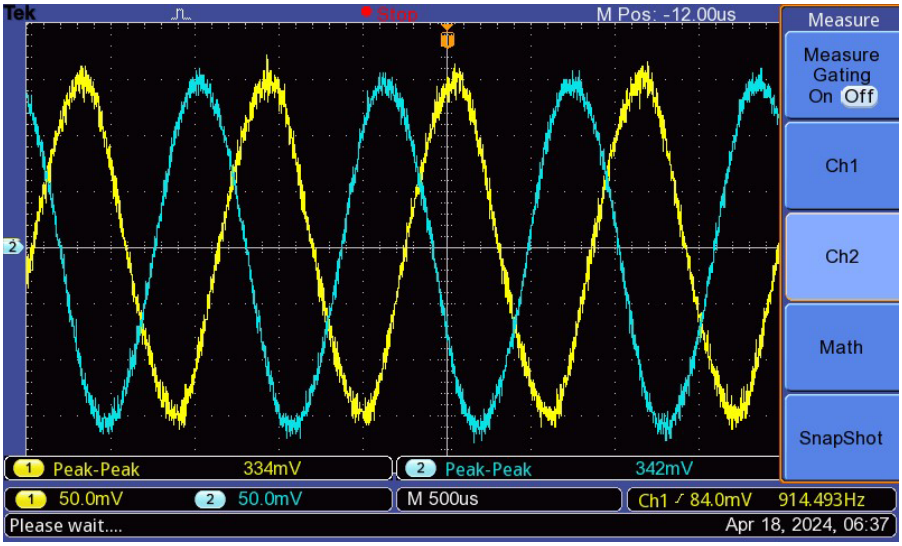

Fig.9 Inductor signal gen vs. voltage across

To ensure these results were correct, an LRC meter was used to confirm our values. For each inductor we received a value of 1.58mH and 1.546mH. With a difference of ~2%, these inductors are well within acceptable parameters to be used as arm inductors.

After ensuring each individual component of the single-phase is working reliably, the full 6-cell MMC prototype was assembled. The entire set-up of the single-phase prototype shown in Fig.10 is built consisting of 3 cells per each upper and lower arms. Incorporating an inductor to the load assisted with smoothing the generated modulated signals to a sinusoidal waveform.

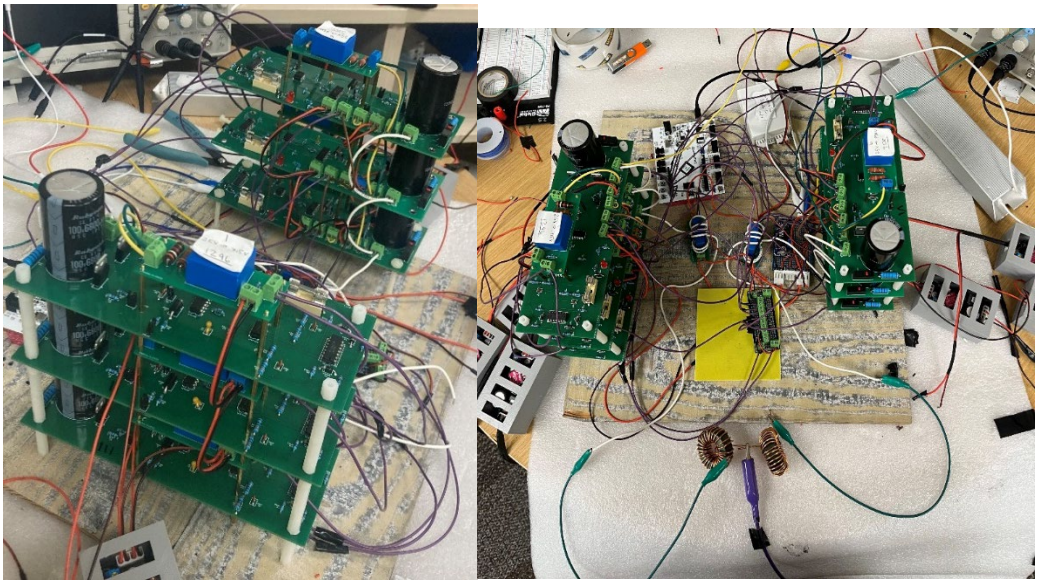

Fig.10 Complete set-up of a single-phase MMC prototype

The prototype is created by stacking cells on top of each other with the voltage sensors on top of the cells they will measure capacitor voltages respectively. Shown in Fig. 10, is the upper and lower arm. A DC bus will be connected to the top of the upper arm and the bottom of the lower arm and will cascade into each other across multiple inductors and output across an AC load. As depicted it is very difficult to maintain concise wiring. One method used to limit the wires is multiple cascades of voltages across each cell. For example, each 15V power supply was cascaded to one another, rather than using three different power supplies.

To control and monitor the system, the PWM signals from the control scheme mainly capacitor voltage balancing algorithm was implemented on the FPGA board, the Spartan-7 XC7S100- the most powerful FPGA board of the 7-series as shown in Fig. 11. This meant there would be no limitations to the size or speed of our program. The board also has a variety of interfaces which were nice to have in the event that we needed them for the future works of this project to implement various control loops such as permanent magnet generator speed, and torque controls or DC-link voltage controller. The requirements for picking our FPGA board

were that it needed to have an XADC, accept a minimum of 6 analog bipolar signals, 2 unipolar analog signals, have a minimum clock speed of 100MHz, and be able to output 6 PWM signals.

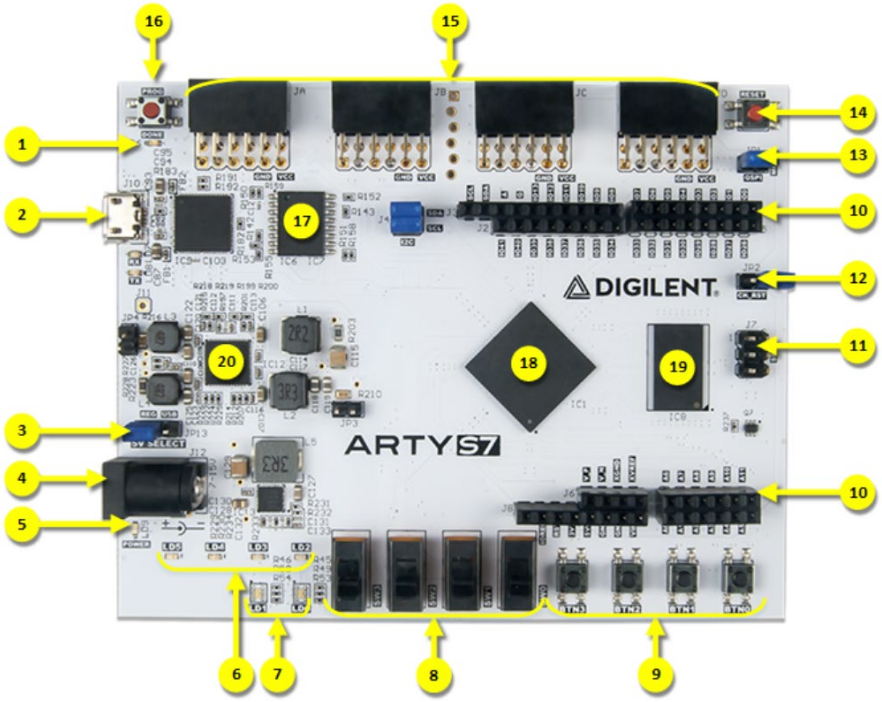

Callout	Description	Callout	Description
1	FPGA programming DONE LED	11	SPI header (Arduino/ChipKIT compatible)
2	Shared USB JTAG / UART port	12	Arduino IDE reset jumper
3	Power select jumper (Ext. supply / USB)	13	FPGA programming mode (JTAG/ Flash)
4	Power jack (for optional ext. supply)	14	Processor reset
5	Power good LED	15	Pmod headers
6	User LEDs	16	FPGA programming reset button
7	User Tri color LEDs	17	SPI Flash
8	User slide switches	18	Spartan-7 FPGA
9	User push buttons	19	DDR3L memory
10	Arduino/ChipKIT shield connectors	20	Analog devices ADP 5052 power supply

Fig. 11 photo of the Spartan FPGA hardware board S7-50 from Digilent and its various components

Experimental Results for the Exemplary AC Loads

The experimental results of this project can be broken down into two sections. The first section is the cell level, and the second section is the full operation of a single-phase prototype.

I. Cell Level Testing

A) LM339 Op-Amp

The main goal of the Op-Amp is to amplify the PWM, boosting the 3.3V peak-to-peak, 2kHz input signal to a 15V peak-to-peak signal. Seen below is the input PWM signal, Fig.12, along with the output of the LM339 Op-Amp, Fig.13.

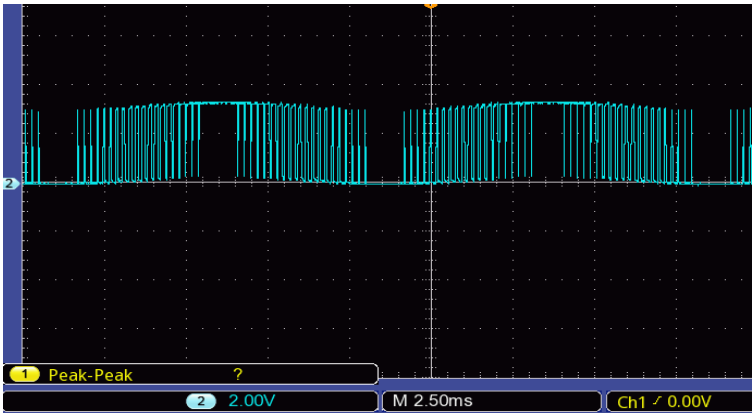

Fig.12 FPGA Input PWM Signal to Cell

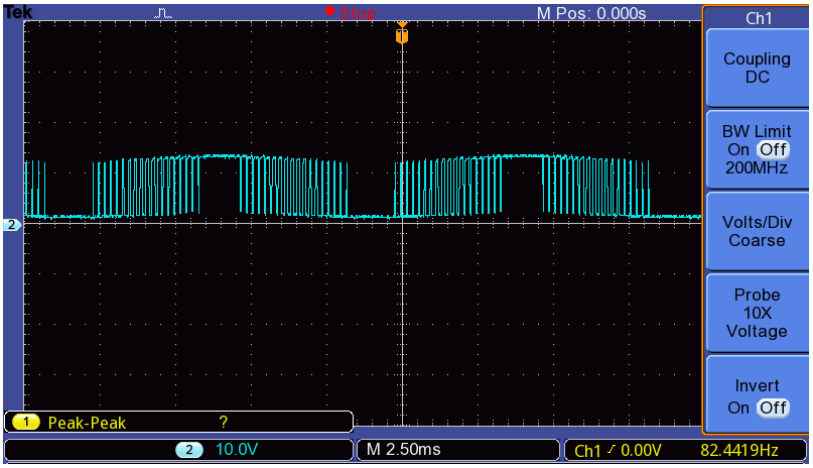

Fig. 13 Output of the LM339 Op-Amp

As is shown in the figures above, the PWM signal is successfully boosted utilizing the LM339 Op-Amp.

B) HCPL2531 Opto-Coupler

Following the cell's structure, the next significant component is the HCPL2531 Opto-Coupler. The goal of this IC, as stated previously, is to smooth and isolate the signal. This is necessary because of the fast-switching frequency inserted into the power section and MOSFETs of the cell. Fig.14 displays the output of the Opto-Coupler, resembling the output of the LM339 closely.

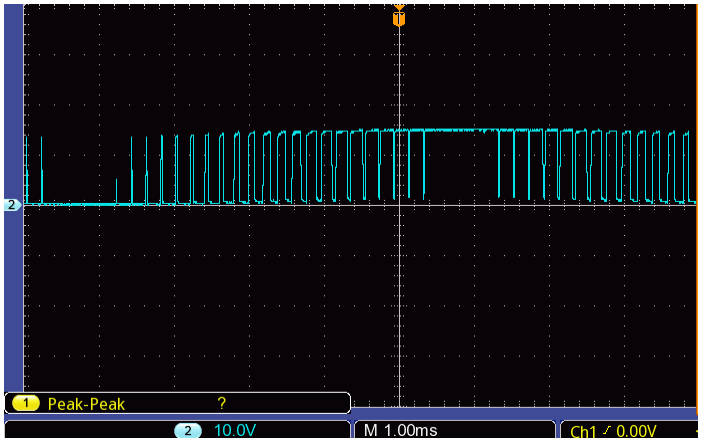

Fig. 14 Output of the HCPL2531 Opto-Coupler

C) IR21834 Gate Driver Board

The following integrated circuit is vital to the task of the cell. As stated previously in the principle operation chapter, the Gate Driver creates two signals, one replicating the original signal and another that is 180° out of phase to control the switching of the MOSFETs. Fig.15 and Fig.16 below display this 180° out of phase operation being conducted.

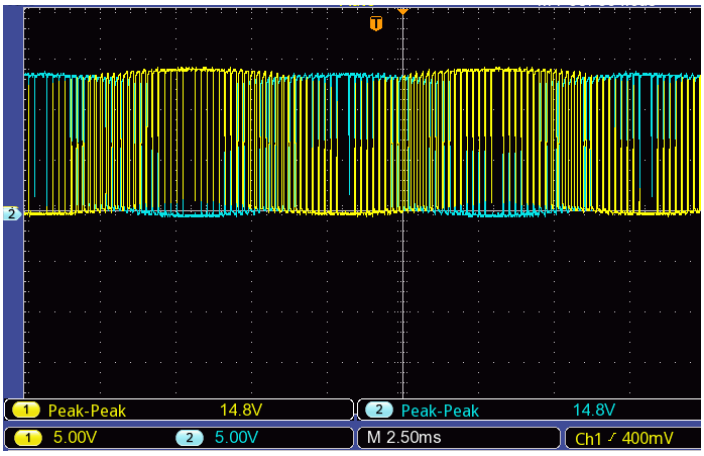

Fig. 15 Output of the IR21834 Gate Driver

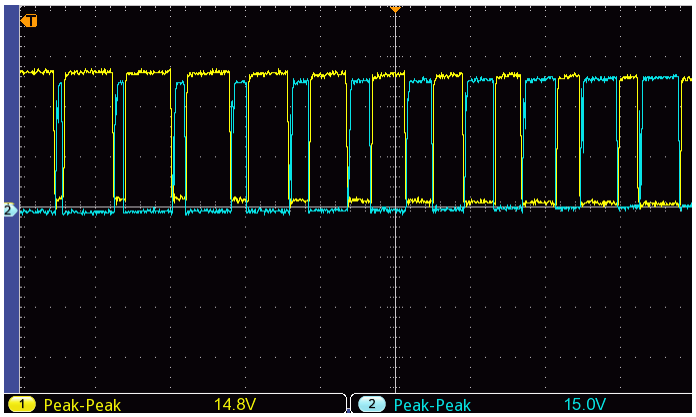

Fig. 16 Zoomed waveform of the IR21834 Gate Driver output

II. Experiments with the complete Single-Phase MMC Set-up

For this experiment in particular, a DC bus was supplied to our system with a voltage of 24V. The system works with the FPGA controller to balance the capacitors around the reference voltage. As previously stated, with 3 cells being in one arm, each capacitor should balance around 8V. Fig.17 shows each capacitor in the system being balanced around this reference voltage. Fig.18 shows the hardware window from the Vivado visualizing all the capacitor voltages; this also shows that the capacitor voltages are on top of each other and the same. In some cases, particularly the bottom arm, there was difficulty in measuring the capacitors. Although correctly reading a balanced voltage around 8V on a multi-meter, when the oscilloscope probes were placed on the output terminal the capacitors would discharge dramatically. Despite this happening, solid outputs were able to be captured across each cell. It can be seen by the ripples in the waves, that this is the FPGA controller balancing the voltage.

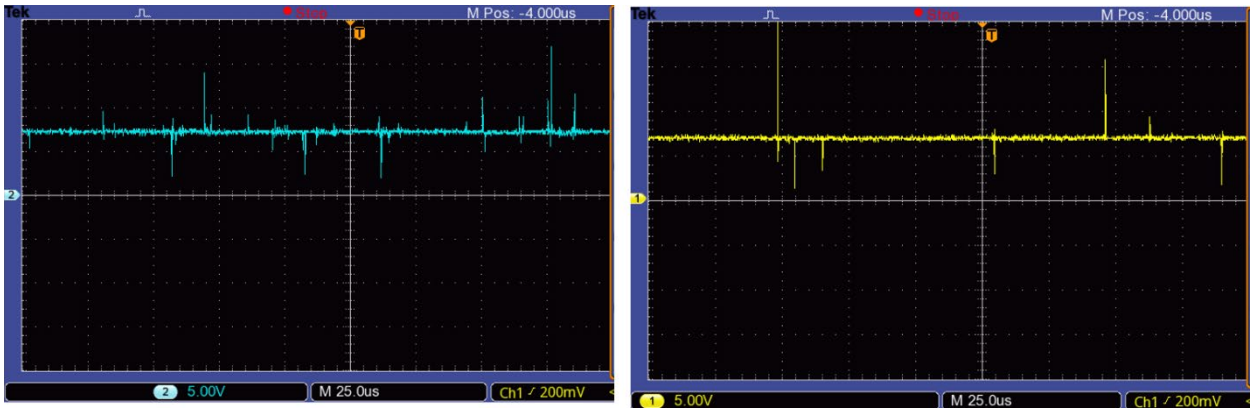

Fig. 17 Capacitor Voltages at Cell 1 of the Upper Arm (Left photo), and Cell 4 of the Lower Arm (Right Photo), capacitors are charged around reference voltage of 8V.

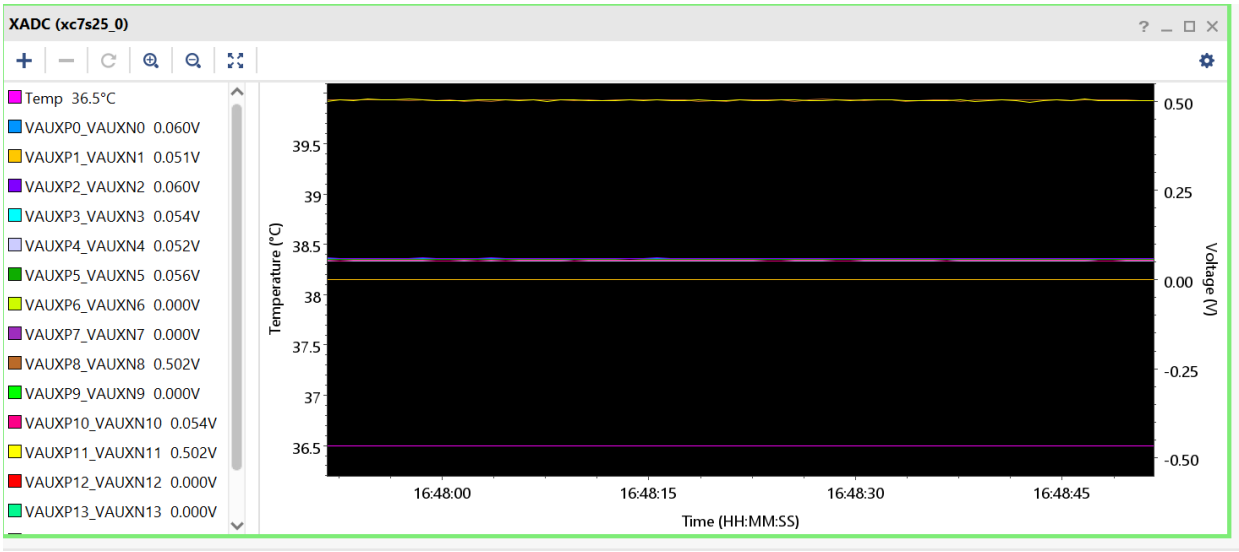

Fig.18 FPGA Hardware Window

Fig.18 shows the bottom multi-colored line along with the readings on the left side of the screen, VauxP0-P5 are balancing accordingly. The top lines are the current sensors being measured checking for direction.

Figs. 19 and 20 show the voltages for the full lower arm and upper arm when an AC motor was used as a load.

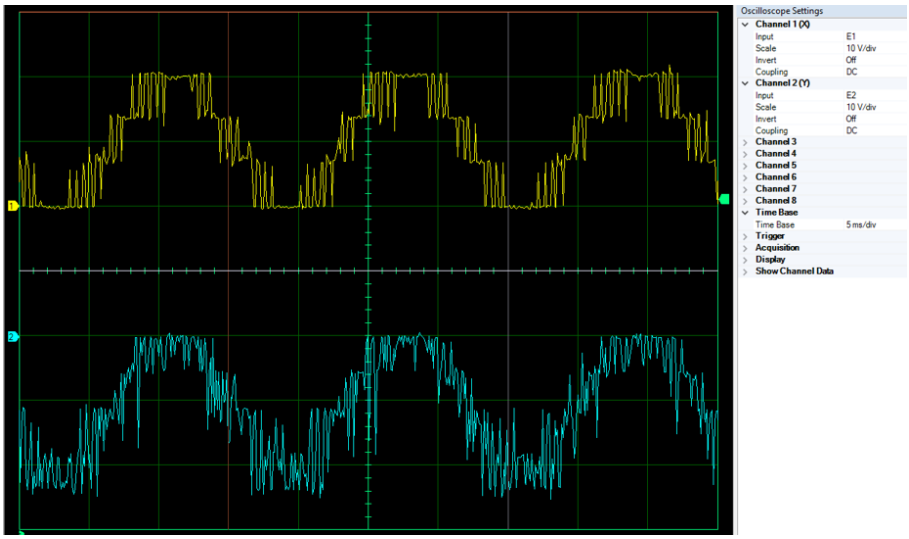

Fig.19 Top Arm (yellow) and Bottom Arm (blue) total voltages

Fig.20 seen below is the combination of the two arm voltages, which is the AC waveform at the inverter output, whilst the bottom wave is the sinewave desired from the MMC output phase

current. As it can be seen, a very smooth sinewave is outputted from the MMC prototype without the usage of a filter. This test was conducted on an AC Motor aca load.

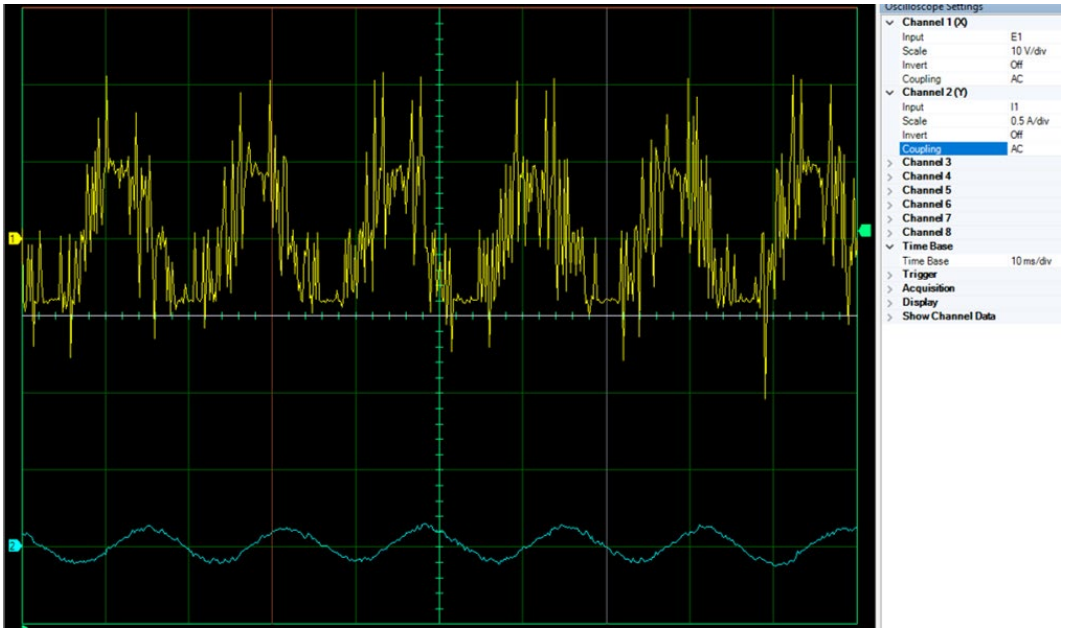

Fig.20 Output Phase Voltage and Current Waveforms for the AC Motor Load

Overall, the results acquired in the prototype testing were reasonable, ultimately deemed successful complying an industry standard such as IEEE-Std. 519 for the power quality and total harmonic distortion (THD) requirements. There are areas that will be improved upon by using better quality wires to reduce the noise inside of the signals, working in an environment with little electrical disturbance, more efficient inductors, a more powerful FPGA board, or improving the PWM strategy and design. Countless mishaps occurred during this process such as capacitors blowing, ICs malfunctioning, sloppy soldering, incorrect wiring, even an FPGA board getting browned out. Regardless, this prototype has accomplished in creating a working cell level design, a functional capacitor balancing algorithm, as well as an operational full single-phase prototype to generate 60Hz AC power.

IV. Development of a 3D Printing Prototype for the Mechanical Sub-system

In this section, the designed 3D model schematics of the key components of the wave energy converter are provided. The preliminary outcome of the small-scale prototype could be used in the early design steps, particularly for component size and ratings, geometry of the buoy and the integration issues.

The 3D plug and Play mockup model creates and animates the energy converter for preliminary testing in water. The experiments using our fully automated pool on campus allowed the team to ascertain the functional behavior of the wave energy converter to refine the design variables, values, and dimensions.

The “Ocean Wave Energy Converter” is a device that aims to transfer energy from ocean waves to compress and decompress air in an enclosed chamber to act as an air pump to generate work that can be rerouted into a turbine to give it enough rotational inertia to turn.

The principle idea of this prototype is to make a way for waves to collide with the discs that would move the reaction rod up and down which would compress the spring attached to the rod inside the air pump cylinder. This spring would then decompress and push the rod back down in a reciprocating reaction. This document demonstrates how a scaled prototype looks. This test was conducted in the kinesiology swimming pool at CSUSM which has the capability to generate artificial waves. The prototype consists of 4 sets of converters attached to a floating platform that connects to miniature turbines through tubes as illustrated in Figure 21.

Before we discuss the results of this test let's breakdown each 3D component and the methods used to create them. Each 3D model was first created in Solidworks then imported over to Tinkercad for further changes and easy access. The two primary printers were used; Fusion 3 and Anycubic Kobra Max as well as two Creality Ender 3’s to speed up the process.

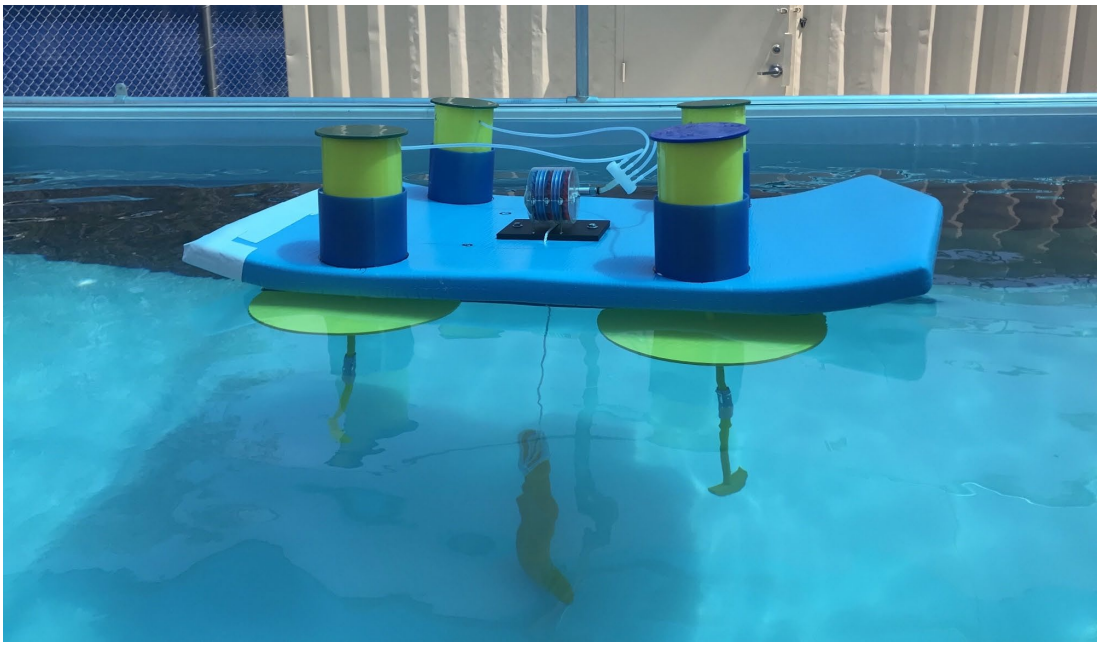

Fig. 21 Overall view of the 3D full prototype

3D component #1 reaction rods

The total height of the rod comes out to about 0.8 meters. However this height is too large for any affordable printers to print this as one piece. So the model had to be split into three separate components, the handle(0.2 m), lower rod (0.3 m), and upper rod (0.3 m). Which are screwed together with small threads. The width of the rods are 13.1 millimeters and are printed with the standard 15% infill.

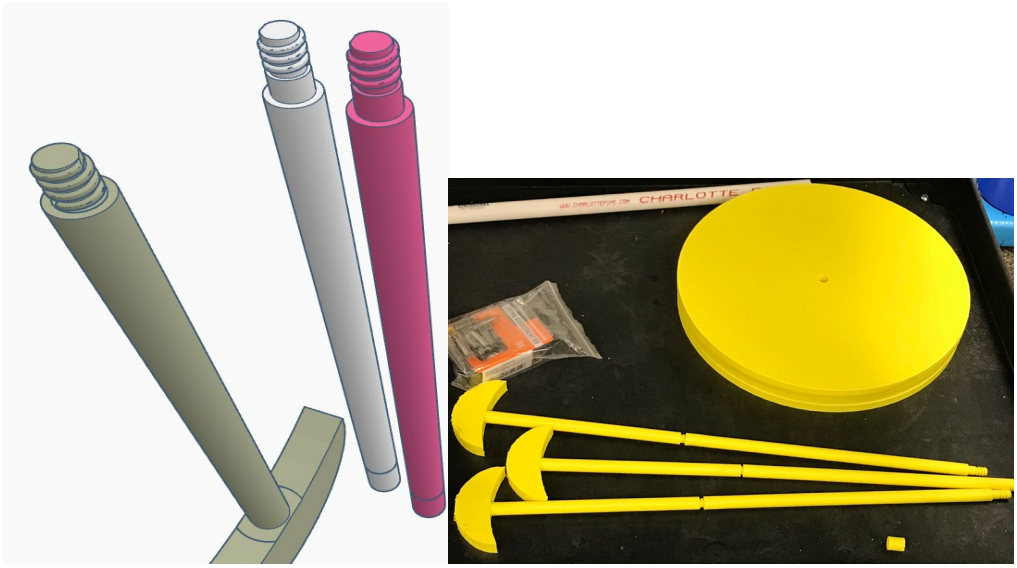

Component #2 Main disc:

The reaction disc is massive at 33 centimeters and 11 millimeters thick, the theory behind this is that its large size will allow it to maximize the amount of energy it could harness from waves. In order to connect it in between the two rods. It rests on top of the bottom rod and is held together when the top rod is screwed on to it.

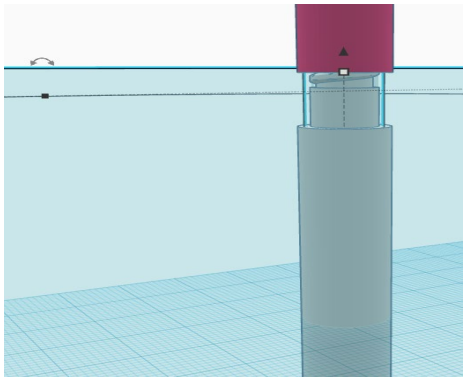

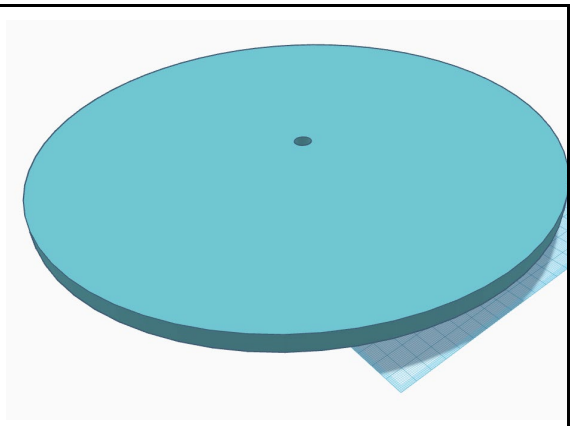

Component #3 Internal disc:

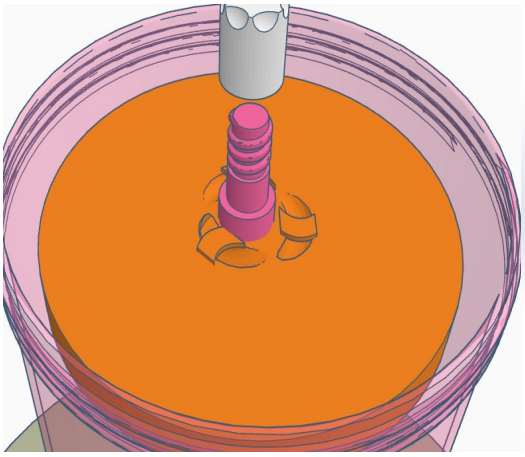

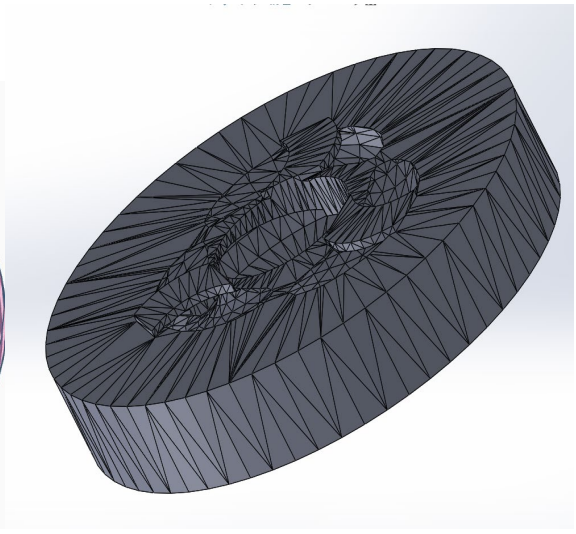

This is the disc that's housed inside of the cylinder. Hooked springs are attached to the three holes in the center which would be attached to the other holes on the cap which have the same mechanism. These hooks are quite strong and don't break even when the springs are stretched to the max limit. This disc will be held in place by a small screw that goes in the center which fixes

it to the rod. These three holes allow the spring placement to be approached from any angle as well as making room for multiple springs to be used simultaneously for a more robust connection.

Component #4 and #5 Cylinder and Cap Version 1

The initial version of these components were very basic and had to be melted together to be connected.

The first real version aims to emulate a bottle cap with threads that can be opened or closed at any time. Initially the threading on the bottle and cap were both in the same direction. With the thread line in the cap holed into the model. It was essentially one large nut and bolt; the hollowed out threads on the cylinder were made 0.2 mm larger to give room for the threads to screw in without getting stuck. For 3D printing this is essential because all printers have a degree of error in their dimensional accuracy. With enough fine tuning and with a very good printer it's possible to get the inaccuracy down to >0.1 mm but it's always a good idea to leave enough room of error for anyone to replicate the print.

While it was functional one glaring issue was still present. The model was not air or watertight, water was leaking out from the point where the cap and cylinder were joined together. The model had to be fully airtight otherwise all air would escape from the chamber and none of it could be harnessed, which would make the whole prototype pointless.

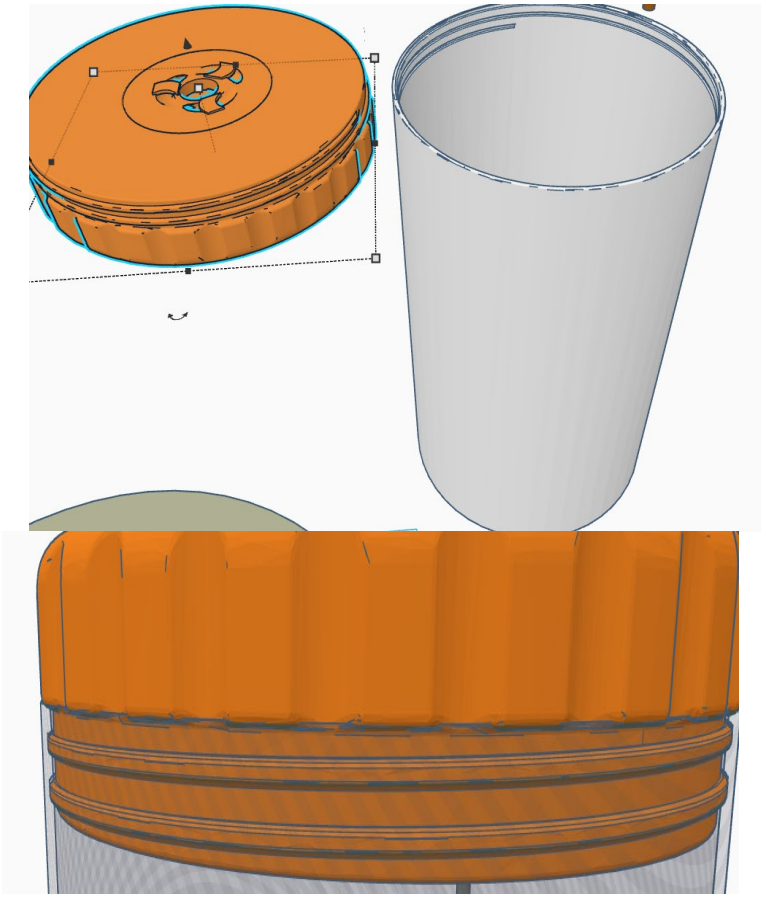

Component #4 and #5 Cylinder and Cap Version 2

For the second version I switched the threads from the inside of the cylinder to the outside of the cylinder. And switched their directions so the cap goes clockwise and the cylinder goes counter clockwise. In order for this to work the sizing of the caps threads have to be small enough to fit in the gaps left behind through each rotation of the cylinders threads.

To smoothly print these threads it was fileted around the corners and the entry was chamfered into a sharp point. The picture below demonstrates these fillets and chamfers. Also while presets for threads exist as a feature in Solidworks, they are intended for traditional screw shapes. The ones for this project had to be built from the ground up because of the unique shape of these models.

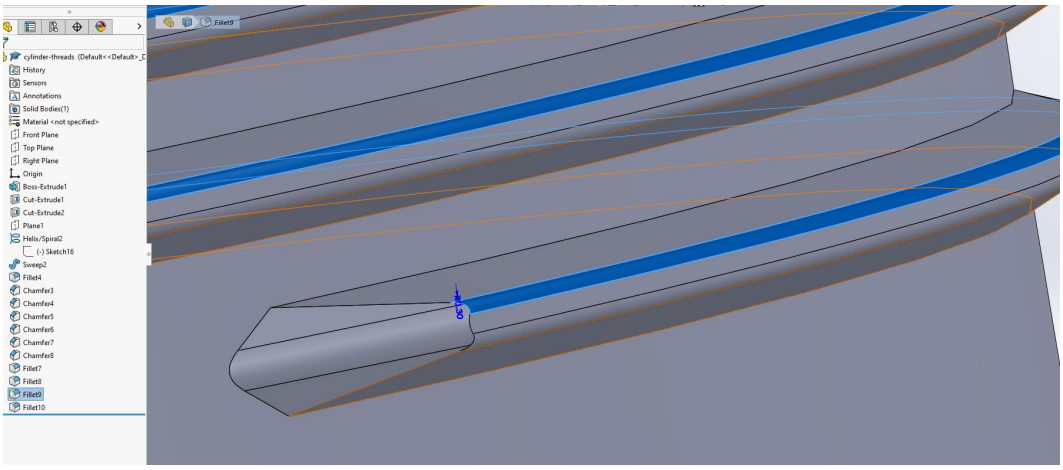

The profile for the threads is described as a congruent trapezoid with a bottom length of 2 mm, to length of 0.75 mm and height of 1.4 mm. The 3D representation of this profile is then swept through a helix until it reaches the top of the cap.

We can then define the revolution, pitch, and direction of a helix and the threads will extrude itself following the path of this helix.

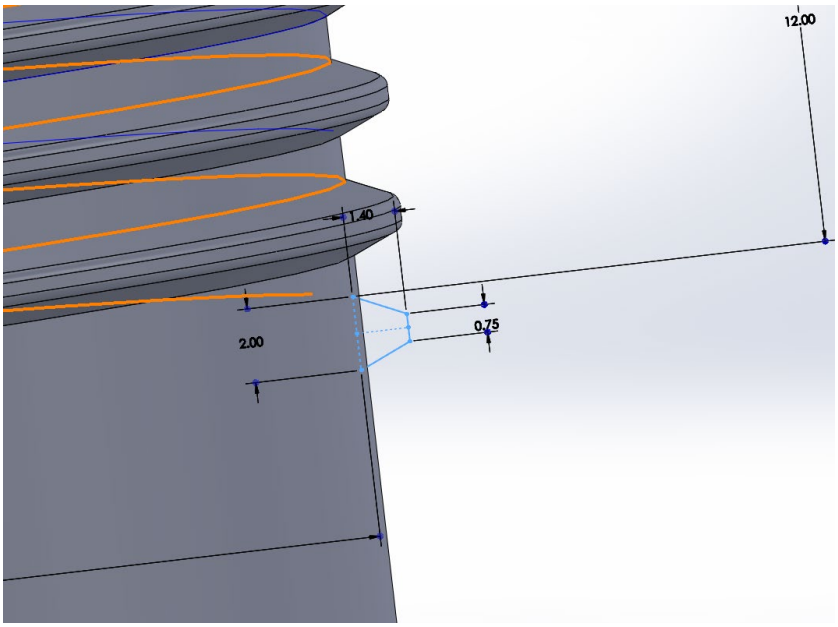

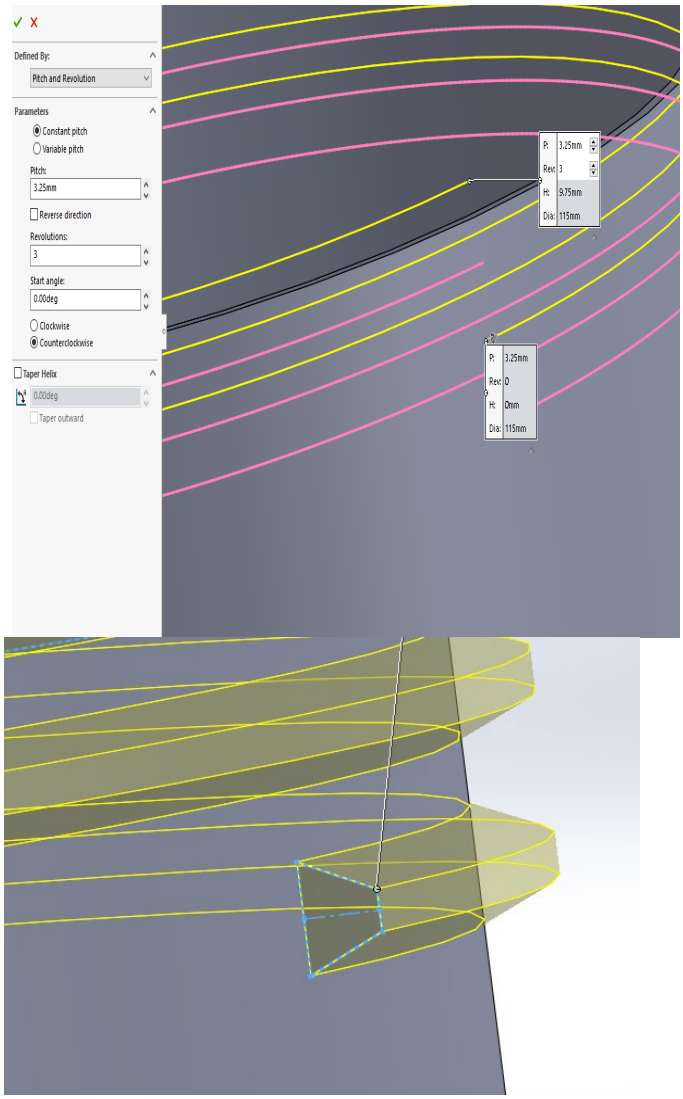

The trapezoidal shaped profile for the cap are set with a bottom length of 1 mm, top length of 0.2 mm, and height of 1 mm. It's less than half the size of the other profile, because the gap between two revolutions is about half the size of one whole thread profile. So these cap threads will twist clockwise into the cylinders threads.

The profile was manually sketched using line and center line tools and placed parallel to the side of the wall.

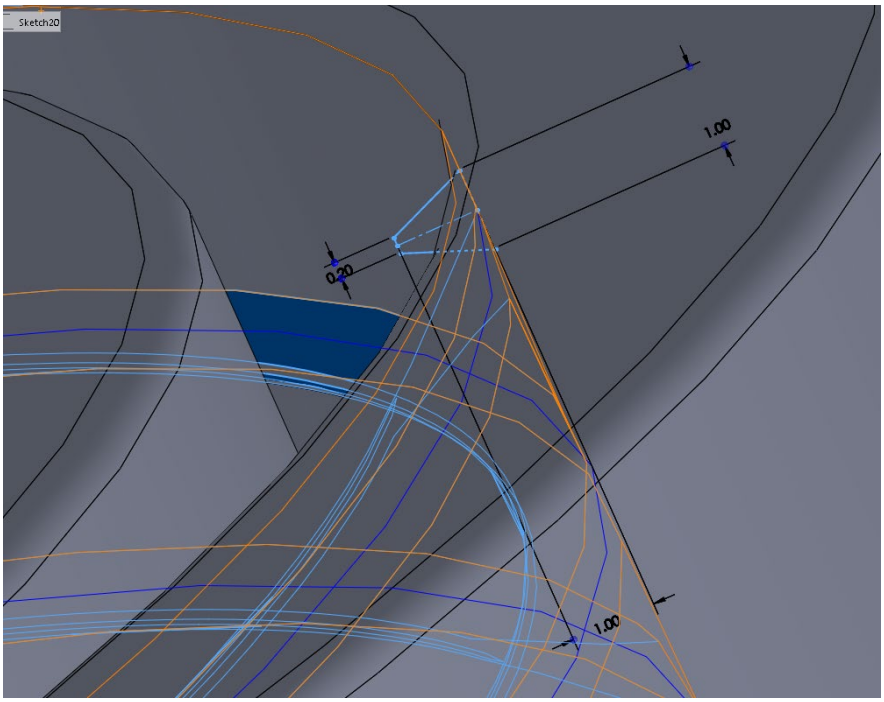

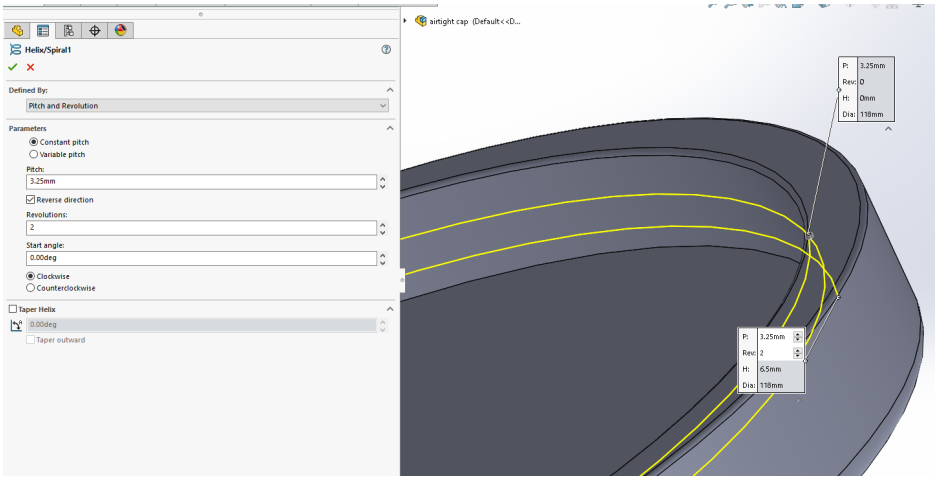

These threads a whole revolution less than the other, this gives ample space to fully close down. In practice, the cap can go about half an extra revolution before it can no longer move at all. It's important that both keep the same constant pitch, which defines the distance before each revolution otherwise they won't be able to fit together. If the cylinder fully tightens then that must mean there is no gap at the top which means no air can escape right? Sadly, when filling the inside with water after a short while there will be leakage. After some investigation it's apparent

that it’s because the top surface of the printer is not perfectly flat which allows for gaps for fluids to escape. This is a limitation of 3d printing technology and not much can be done to amend it.

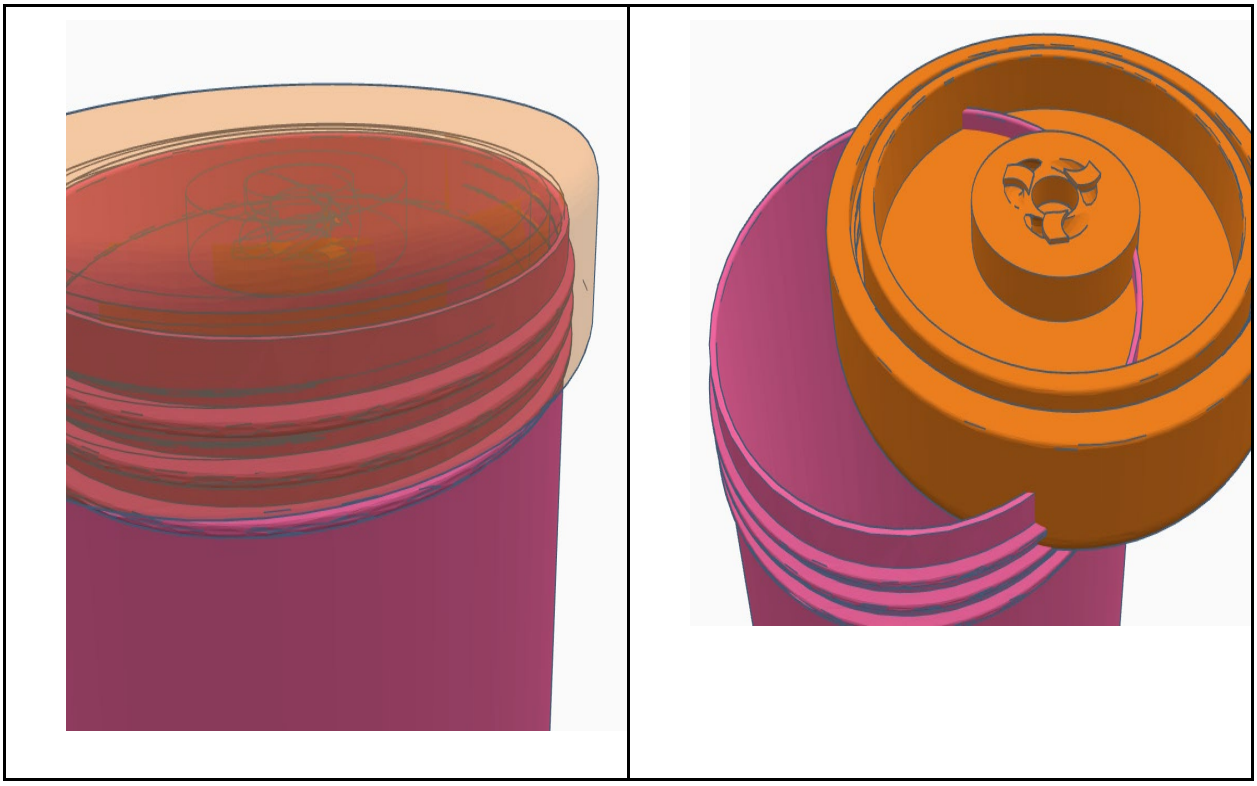

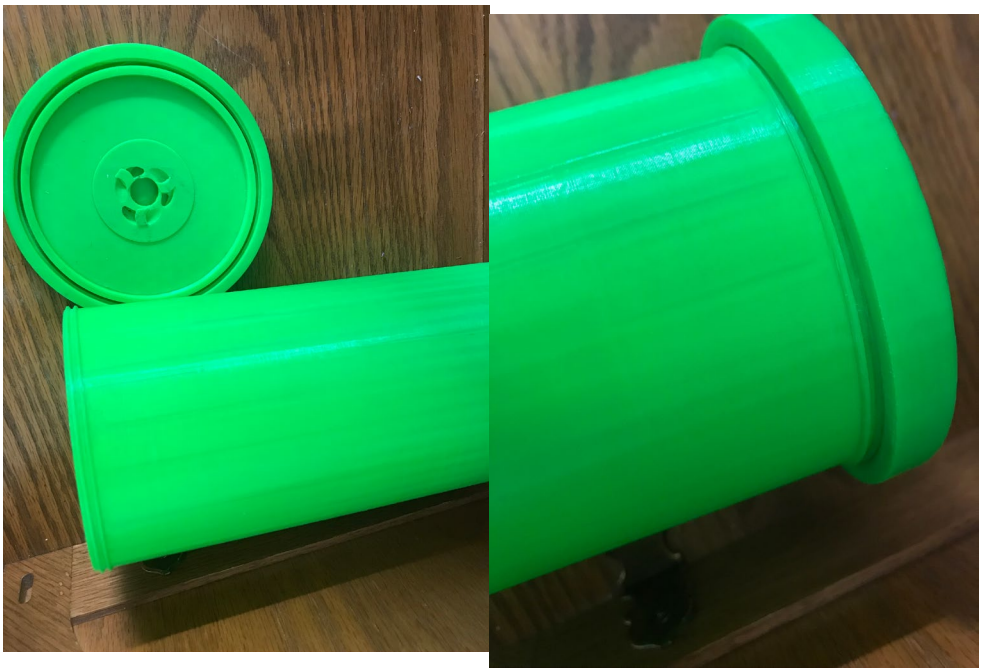

Component #4 and #5 Cylinder and Cap Version 3

The last attempt made was to get rid of the threading and experiment with a new system. This iteration uses a rubber gasket to close the two parts together.

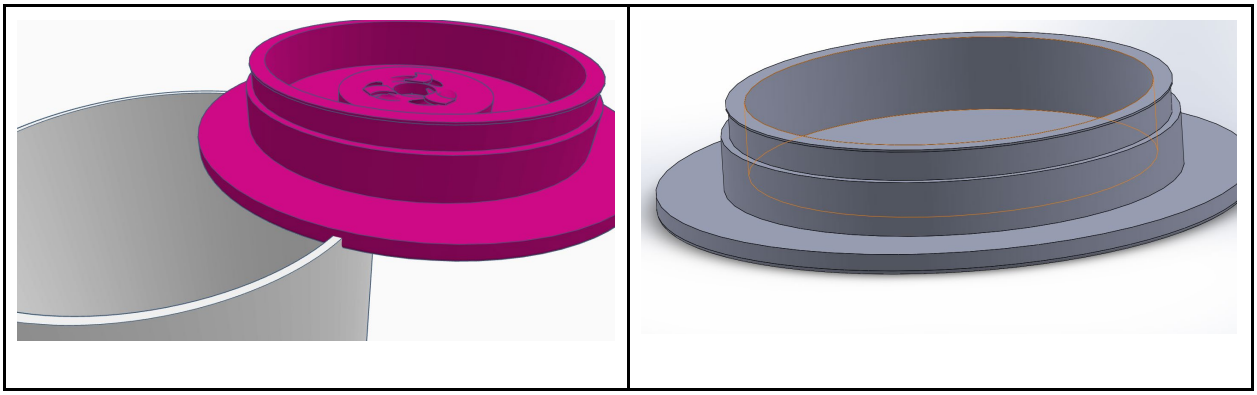

This is a much simpler design concept: simply stretch the gasket into its position and close them together. Would this work? Unfortunately not. It gives the illusion of a watertight fit. But after some time passes, small amounts of water leaks through. So it would seem that the project had hit a road bump, 3D printing is not usually meant to be watertight. It's too difficult to attempt to create a fully watertight model that works right off the print bed. However, with the right post processing it's possible to do so. In hindsight with the right post processing even the first version would have worked.

In this case the product that put this project back on track was "Flex Seal" A liquid rubber sealant product created by the legendary Phil Swift. After twenty four hours the applied flex seal produces a real watertight barrier. The use of this product overcomes the major design challenge that made this project impossible to complete. By covering the entrance point of the cap and cylinder with flex seas so liquid was able to escape even after being left for a week filled with water.


4

Slicer Settings:

The Cura slicer was used for these prints, Slicers work by converting the STL File of a 3D model into G-Code which are instructions that the printer is able to read and follow through in extruding its filament into a specified shape. For most components in this print the standard 0.2 mm layer height and 15% infill was used.

However, the cap and cylinder use special settings curated to make the surface watertight and prevent leakage through the material itself.

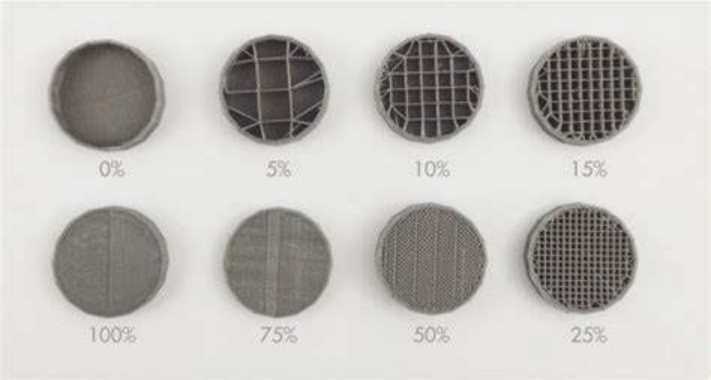

Filament based 3D prints are typically not fully filled in; rather, it has an outer shell and the insides are filled in a pattern that is enough to form the model while using the least amount of material and time. Only the initial bottom and top layers are fully filled in. The bottom layers are fully filled so that the model properly sticks to the bed and has a strong foundation.

It’s common knowledge that bumping up the infill settings produces a more structurally sound model at the cost of time and material. One might think that a 100% infill would fully fill the inside, however in most cases that is incorrect, the infill pattern is still there, it's just really small.

The solution is to actually set the infill to 0%! And from there manually increase the wall and bottom/top layer count to cover the entire model. By doing so we trick the slicer into thinking that it's always printing the bottom layers.

Demonstrating the following with a cap model:

This is what the model looks like under normal settings, the walls are just hollowed in on the inside. Even a small cut or hole on the top layer would reveal the infill patterns.

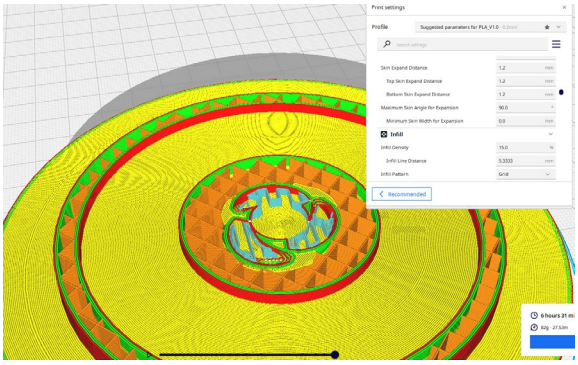

At 0% infill the walls are completely hollow on the inside, printing it as is would be unfeasible and the print would collapse without infill to support it.

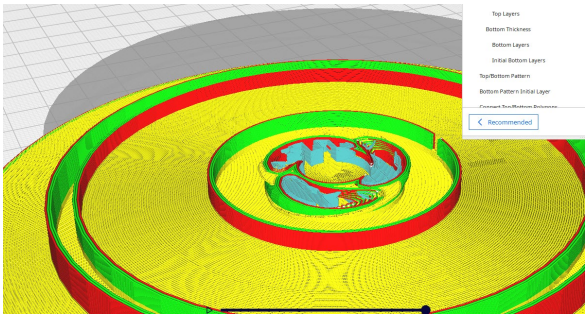

But by changing the wall and bottom/top layer count to its max count we've created a solid piece with no gaps. The walls are denoted by green lines in this preview when comparing it to would normally print the gaps between walls, we see that having more walls make a far more rigid structure.

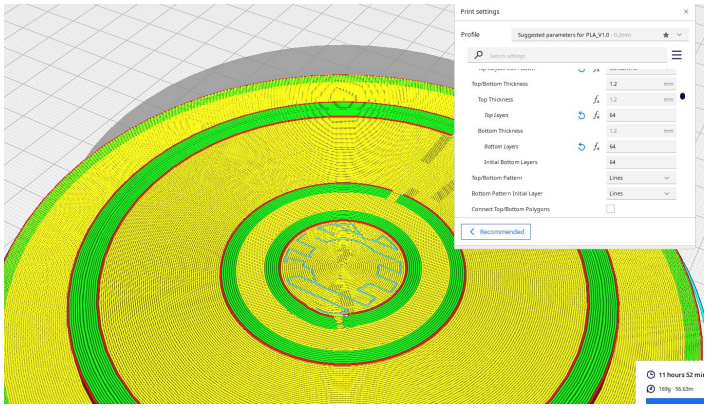

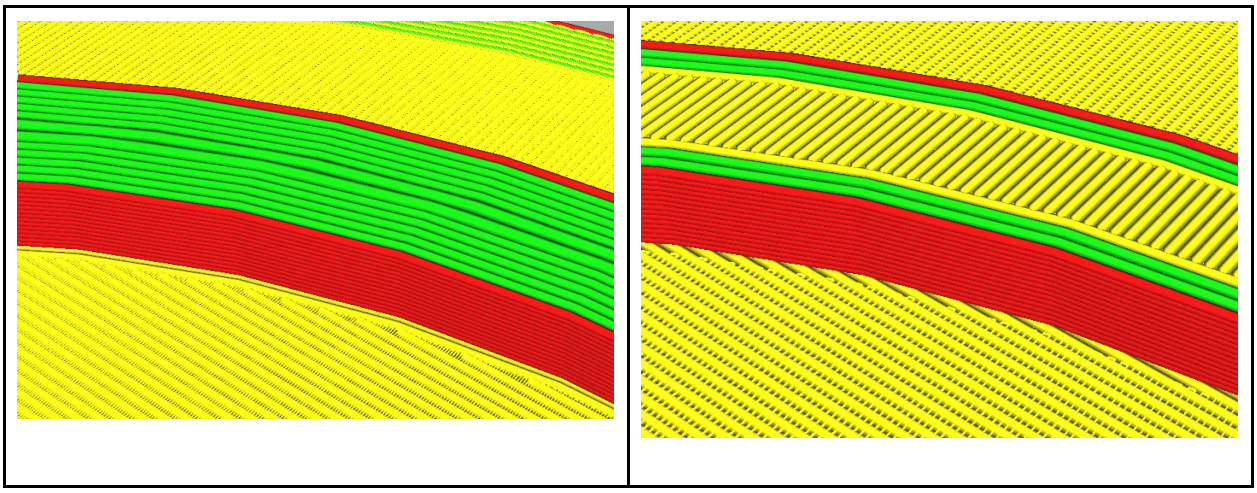

Left: A wall structure with a maxed out wall layer count, each wall is printed at one go of the printer without lifting the nozzle up which creates a more uniform surface with little gaps.

Right: A standard print at 100% infill. The wall count is only a few layers thick and the inside is filled in with infill material, while taking less time overall this method would leave many microscopic holes for air to potentially flow out from.

Exploring Other Waterproofing Methods:

- **Vase mode:**

  When printing a cylindrical circle the nozzle normally draws a single line, lifts up and goes back to a starting point before printing a new layer. This tends to cause seams and gaps each time the nozzle is lifted up and repositioned. One experimental method to remove these seams is to print in Spiralize Outer Contour or “vase mode”. This prints one single wall in a spiral pattern without ever stopping the extrusion, this method is analogous to writing in cursive.

  While it does produce a wall with no imperfections, unfortunately this mode is only able to produce a shape that's only one wall thick which is too fragile for our goal. Luckily the slicer setting used to define the cap is technically a pseudo or fake “vase

mode" because it produces all the effects of what vase mode does while allowing for more walls. The difference between vase and standard mode is demonstrated in the image below. Enabling the mode will automatically get rid of any roofs and reduce the wall count to one If there were no limitations on wall count vase mode would have been a very useful tool to utilize.

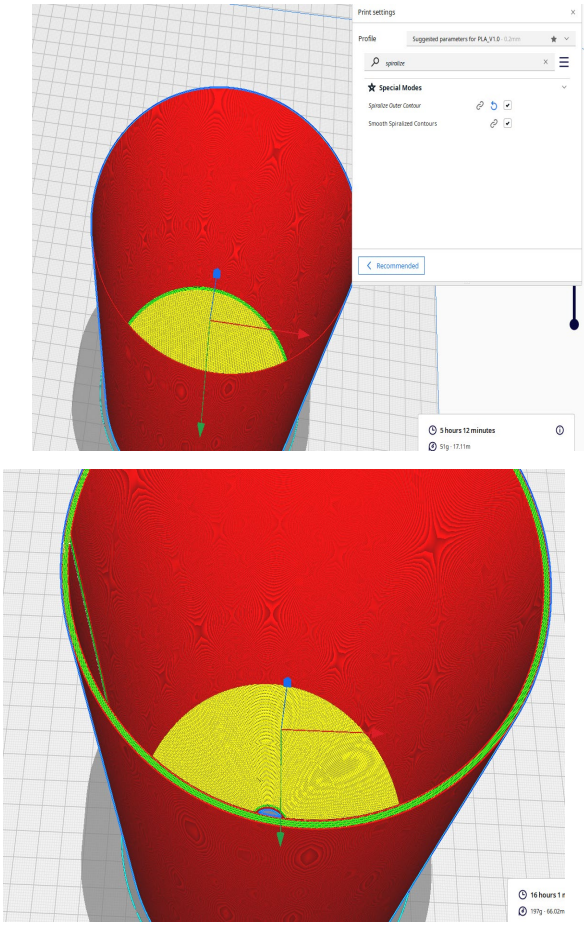

- **Extrusion Width:**

This setting defines the amount of filament that gets extruded out from the printer. One possible method to create watertight walls is to over extrude your model by setting the flow rate to 120% or more to make the layers overlap with each other and close any gaps. However this is a rather rudimentary method because it tends to cause noticeable blobs and stringing of the material which prevents the threads/gaskets from properly working. Over extrusion can also be achieved by swapping to larger nozzle size for these

prints 0.4 mm nozzle was used but a 0.8 mm nozzle would produce similar effects to over extrusion.

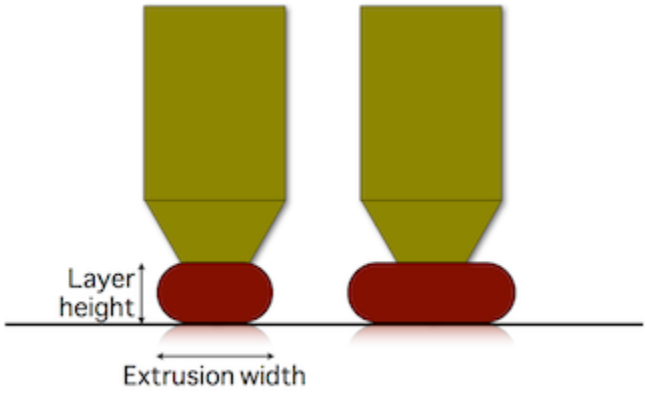

- **<u>Epoxy Resin Coating:</u>**

This is by far the most effective post processing method at creating watertight prints. An epoxy coating consists of a solution A and solution B that are mixed together in a 2:1 ratio, after a few hours this solution will dry and after 24 hours it will fully cure. This coating will fill in any gaps and form a clear, glossy surface that is totally air and water-tight. This was tested on a print that was only a few walls thick and even after a week there was zero leakage along the walls, showing its effectiveness.

For the sake of safety this should be done in a well-ventilated area while wearing gloves any coating that gets on your skin or eye should be immediately washed away. The coating should also be uniformly brushed across the surface and for maximum effectiveness it should be done on both the inside and outside walls.

The pictures above demonstrate the smooth glossy finish achieved by epoxy coating. It removes visible layer lines and makes a unified surface. It also protects the model from physical damage and reinforces the strength of the spring holders. It's very important to remove any supports before coating otherwise they can’t be removed and not touch or move the print before the coating dries or the layer will be ruined.

Assembly of the 3D Mock-up Model

The assembly of the prototype was a fairly straightforward process.

Appropriate sized holes were cut into the foam board and was covered with a PVC pipe that was cut and sanded to the correct size. These pipes provide a straight pathway for the rod to move in and out from. The cylinders were then glued on to the platform and a hole was drilled into them to insert tubes that connect to a fan in the center. Careful alignment was required to make sure the hole in the cylinder aligns with the one in the foam board other side the rods would get stuck. And since this is being glued together with flex seal anything glued together would be close to a permanent connection so there is little room for mistakes. But if the misalignment was small it could be fixed with sandpaper.

In addition, WD-40 lubricant is used to insure the rods can smoothly move in and out without any friction which would cause significant losses in efficiency.

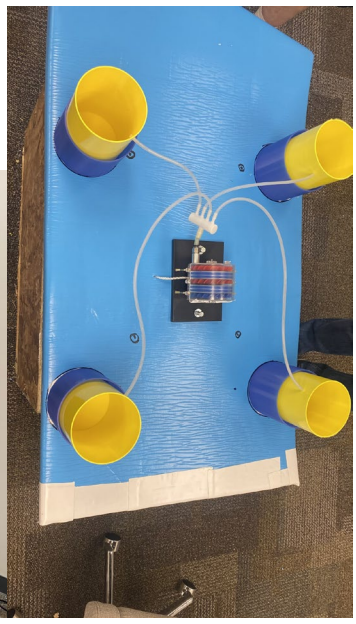

Water Testing from components to full prototype

Initial testing in November showed that the spring does indeed move up and down in a reciprocating reaction. The goal now is to see if this scaled up prototype is able to harness this reaction and turn the small turbines with its compression and decompression of air.

The test was conducted in the kinesiology CSUSM wave pool and at low wave strength the rods were moving up and down as intended, however at strong speeds some things went wrong.

First the top of the cap disconnected from the cylinder. It would seem that the gasket by itself was not enough to hold the assembly in place because as the rod moves up it pushes on the cap and slowly pops it out. The solution to this is to simply revert back to the version that uses threads instead of a gasket. Unfortunately epoxy coating and flex seal was only discovered as an option after we moved on from the version that uses threading. In this rare instance the older version would have worked better than the revised one.

The second issue was that after some time the large disc stopped moving entirely and settled down at the bottom. This was because the inside of the disc started to get filled with water which made it very heavy and removed its buoyancy. This can be avoided by switching to non-water absorbent filament or also coating the discs in epoxy coating but this was neglected until we could see that it did cause problems. Furthermore, the discs in general were too large and heavy for this pool.

The third issue was that the joints that connected the rods together were too fragile which resulted in them snapping off at strong wave settings. Looking back up at the mechanism that holds the two rods and the disc together (component #2), it's clear that the thinner midpoint that the disc rests on is very fragile and is the cause for it to snap because the heavy disc rests of the

bottom rod puts a lot of weight on it such that it breaks off. The way to fix this is to make the connection point thicker rather than thinner than the entire rod. That way it can handle the pressure, and the way the disc is held together by the rod needs to be changed such that the threads are able to screw into the hole all the way. As it currently stands there is a thin section of the threads that are not able to be inserted because its whole length is slightly smaller than the thickness of the disc. It should be possible to use a feature called selective infill to keep the rest of the rod at low infill but have its screws be printed at 100% infill for maximum strength.

As of now there is no time left to enact these changes and perform another test. But that's something that can be attempted during summer and MECC 2024 which we aim to be as part of. The team is confident that with one more test we will get this prototype to function as intended.

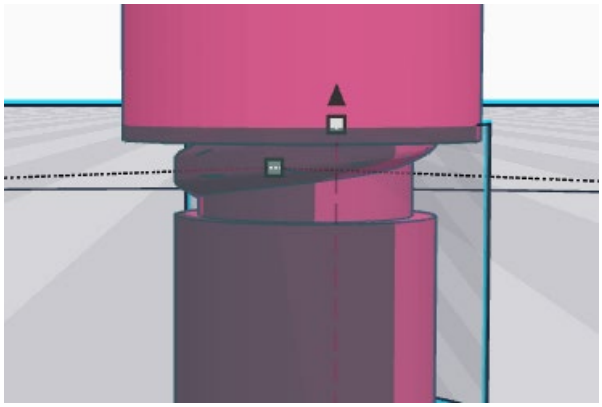

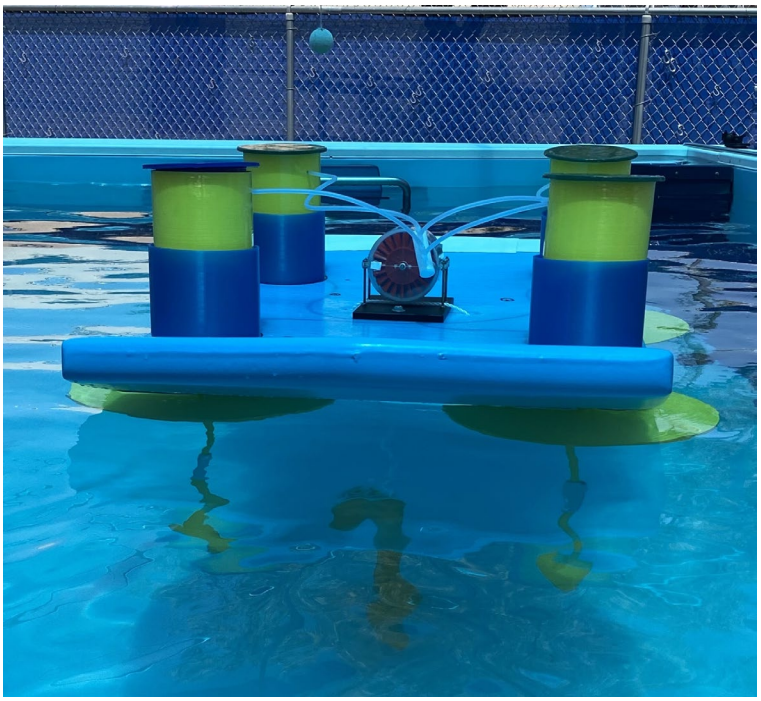

Our initial test was conducted in November 2022 that was only one small scale air-pump set, as shown in below photo, while the second test was performed in April 2023 focused on upscaled version closer to our intended vision.

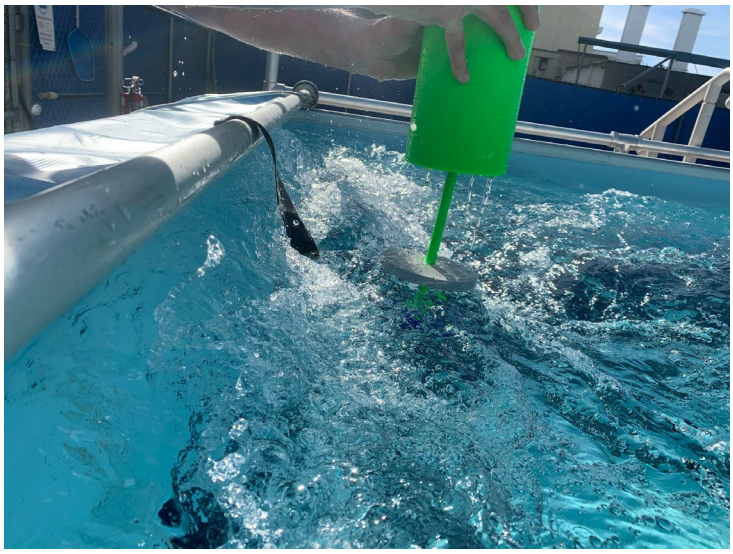

While more refinement is required to verify whether this setup has the ability to generate enough energy to turn the turbine, the tests show that this prototype at least works mechanically as a wave-actuated air pump. In that it does have the ability to compress and decompress the springs through reciprocating function of the reaction rod/disc.

As it stands the current prototype fails the durability and safety test due to critical failures in its joints and performance fails in strong wave conditions.

Lessons Learned from Preliminary Water Testing

While arguably the simplest part of the MECC challenge, the build and test phase of the project vastly improved our personal 3D printing knowledge and led to the discovery of many helpful tools and tricks that can be used in future projects. The ocean wave energy converter is no longer just a concept but something physical we can see and touch. With only a few more weeks worth of work the 3D printed model can be perfected and next semester we plan on moving on to an actual metallic version.

It should be emphasized that the dimensions indicated in this report are estimated and should be adjusted based on extensive tests in water tank to maximize use of best materials, in particular carbon fiber materials related to this specific application.

Harnessing wave energy is within our reach!

V. Business Plan

A) Performance Metrics

The physical attributes of the WEC combined with the most likely areas of applications contribute to a high level of cost competitiveness and provide strong incentives towards the commercialization of the wave energy converter.

Average Capital Expenditure (ACE), a metric for measuring the converter effectiveness, is a ratio of 1) Average Climate Capture Width (ACCW) meters, and 2) Characteristic Capital Expenditure (CCE). ACCW is a measure of the effectiveness of a wave converter at absorbing power from the incident wave energy field expressed as (kW/m) of the wave crest. As such, the capture width is a crucial optimizing parameter. Capture widths will be determined through the analysis of experimental data obtained from testing in water. CCE is a measure of the capital expenditure in commercial production of the device structure. It is computed as a product of a) *Total Surface Area* (m^2), b) the *Representative Structural Thickness* (m), c) *Density of Material* (kg/m^3), and d)*Cost of Manufactured Material per unit Mass* ($/kg). All these characteristics play into making the harvester feasible for large-scale manufacturing and to increasing capital expenditure to exceed the current metric of 3m/$M.

Considering the current state-of-the-art limitations, there is a need for a technology that is modular and scalable so that the designed wave energy converter can be assembled as a plug-&-play manner and deployed rapidly. Modularity offers many advantages that, while manufacturing costs can be minimized, the operation and maintenance costs could also be substantially decreased by enabling quick replacement or repair of failed components. The ease of manufacturing using advanced 3D printing, ease of assembly, transportation, and deployment, ease of repair, and the fabrication of spare parts on demand all contribute towards a technology that satisfies the criteria for technology viability from economic standpoint.

Based on the WEC concept illustrated in Figure 1, the definitions and variables which are important for performance metrics are given in below Figure as

$$\text{Average Climate Capture Width } ACCW = \frac{Power\ absorbed}{Power\ radiated}, meters$$

Characteristic Capital Expenditure (CCE) is expressed in millions of US$ that includes the manufacturing cost, transportation and deployment costs, and all costs required for certification. Therefore, the Average Capital Expenditure (ACE) can be calculated by

$$\text{Average Capital Expenditure, } ACE = \frac{ACCW}{CCE}, meters/US\$M$$

Let's follow basic performance metrics for 100kW design rating to better understand it. By assuming Radiated power of 33.3 kW/m and for the WEC prototype absorption power of 100kW (rated power), the Average Climate Capture Width (ACCW) in meters can be obtained as:

$$ACCW = \frac{100}{33.3} = 3\ meters$$

Thus, Capture Width is equal to 3 meters.

Characteristic Capital Expenditure (CCE) in millions of $US includes Total Surface Area, Representative Structural Thickness, Density of the Material, Cost of Manufactured Material, and additional costs that capture the end-to-end cost of deployment and certification.

Assume the WEC cost as One Million US$, the ACE is

$$ACE = \frac{ACCW}{CCE} = 3\,m/\$1M$$

It should be noted that the state-of-the-art Average Capital Expenditure (ACE) is within (2m-3m)/$1M

The doubling of the current state-of-the-art ACE metric to 6m/$M, offers significant competitive advantages.

Since the focus application of this WEC has been desalination plant powered by this WEC, our team has conducted a preliminary analysis about power saving or improving the energy efficiency of the considered Carlsbad desalination plant in California by deploying the full-scale prototype of the envisioned WEC. An estimated numbers for this desalination plant are: $5 cost per 1000 gallons produced clean drinking water, thus for Carlsbad desalination plant with capacity of 50 million gallons per day [8], the daily expenditure of $50,000 electricity bill is expected. As a result, annual expenditure of $18.25 million is calculated for this plant to pay to the utility which is San Diego Gas and Electric (SDG&E) company.

The estimated cost of manufacturing of this WEC for Carlsbad desalination plant is $5 million and compare the 10-year electricity bill saving of $177 million with cost of manufacturing this technology it is much cost-effective solution. Besides cost saving of the electricity consumption, the plant is less dependent on the utility power grid that could be congested during summer or heat-wave season in southern California region.

B) Industry Outlook by Technology and Application

Based on many published business studies and reports on the projected global wave energy market, it is found out that substantial larger market could be achieved over the next 5 years as roughly 3 times market growth compared to 2015. Among main driving factors, the power generation innovative solutions are expected to be the most significant portion of wave energy market, by application, during the forecast period to a main emphasis on electrical energy generation deploying renewable resources. Many studies foresee realization of offshore wave power plants with power ratings up to 25kW or 50 kW in the years ahead. In shower waters with wave heights of 2-4ft such as more coastal areas, wave energy exploitation can produce about 10kW power.

Considering the location of the wave energy market, shallow water areas are expected to be the largest and fastest growing market over the next 5 years. The operational efficiency of near shore installations is found to be better than onshore facilities in many cases, giving the developers an excellent opportunity to grow further in the future.

It is expected that there will be maximum adoption and implementation of wave energy conversion devices owing to the presence of many companies working in the research and development of wave energy converters.

Another growing application is with regard of rethinking the south and southwest geographic region is being suffered from water scarcity and long-term drought continues to negatively impact the region. Therefore, there is huge demand for solutions that providing continuous supply of drinking water to impacted communities. Notably, ocean desalination applications in Southern California have directed industry attentions and the California Coastal Commission to work on practical solutions to deal with water issues. For example, the desalination plant is in operation in Carlsbad, CA which is the first water treatment plant in the state of California

serving 400000 people in San Diego County. In early 2022, Governor of Arizona announced $1B investment on solutions for implementing effective water desalination plants [13].

Off-the-shelf components, including pistons, pumps, and power generating equipment and hardware establish a market chain of suppliers enabling the manufacture and commercialization of the proposed WEC concept. The market potential including a survey of potential vendors need to be studied as part of the Technology Readiness assessment explore advancing business opportunities for offering off-grid utility and emergency services around the globe. There are immense opportunities for island nations throughout the world to employ this concept for creating sufficient energy mix with conventional power generating sources. Recently, Puerto Rico, and the U.S. Virgin Islands experienced the worst power outages in U.S. history.

Oil & Gas companies can benefit a lot through applying these concepts, securing an energy source for oil floating platforms during an emergency circumstance.

The concept fits very well in alignment with the coming Offshore Wind farms, as our buoy and generators can be deployed in between the major offshore-wind turbines that are relatively far apart and the generated electricity could be merged into distribution collector in wind farm electric distribution network has already been deployed either offshore or on land.

Other notable applications of this technology beyond feeding power to the grid are supplying power to coastal charging stations for ferries, and ships as visualized in below figure.

VI. Summary and Future Works

Our team developed the envisioned Wave Energy Converter using 3D prototyping and the participation in this competition allowed team members to expand their knowledge on basic modeling, simulation and building 3D models for marine applications to validate a studied design concept. Among the available and existing studies, promising simplified modeling techniques show sufficient overall performance analysis compared with complex and detailed modeling cases. The team aim has gained enough knowledge on 3D modeling and printing to build the small-scale prototype focusing on system level issues for initial proof-of-concept in water tank.

The second part of this project focused on hardware development of the power electronics converter as an Inverter based on the modular multilevel converter (MMC) topology. This part was conducted involving three students with major in electrical engineering as part of their senior capstone project.

For the future work and potential topic in next year competition, our team will start conducting sets of experiments using a second prototype which some components are build with metal to further adjust the design parameters based on lessons learned from testing results of a first prototype. Specifically, design considerations with inclusion of different ocean/sea conditions and wave profiles as discussed in [14] supported by experiments will be scheduled accordingly.

The intention of each team member in this phase of our project was to gain more knowledge in broad area of emerging marine applications for bring Marine Energy, particularly wave energy converter knowledge and possible industry connections to our university through creating an opportunity and demo where junior students can gain hands-on experience on this subject matter.

Most team members and anticipated new team members are going to take courses named ‘’Power and Renewable Energy Conversions’’ and ‘’Control systems’’ in addition to the senior Capstone project in the Fall 2023 semester with the team faculty advisor. The power electronics design interfacing with the generator and basic control functions will be the subject of the students’ final project for abovementioned courses. This is an effective way to incorporate the results of our team efforts in MECC 2023 into a course curriculum.

Having identified a local company named *Breakwave Energy Engineering*, we are making a progress to sign industry agreement and partnership with this company this summer. *Breakwave Energy Engineering* has agreed to build an industrial scale prototype of our design and the plan to perform a water testing in Lake Erie, Pennsylvania in real-world application. We strongly believe that this opportunity will enhance our learning in particular related to manufacturing aspects of this technology. This will be our future work aiming to participate in MECC 2025. The team is also working with the team faculty advisor to prepare a paper based on the hardware development of a MMC-based PTO system to be submitted for the Journal of a Marine Science and Engineering this June.

VII. References

[1] X. Zhang, X. Tian, L. Xiao, X. Li, and L. Chen, "Application of an adaptive bistable power capture mechanism to a point absorber wave energy converter," *Applies Energy Magz., Elsevier*, vol. 228, October 2018, pp. 450-467.

[2] LiVecchi, A., A. Copping, D. Jenne, A. Gorton, R. Preus, G. Gill, R. Robichaud, R. Green, S. Geerlofs, S. Gore, D. Hume, W. McShane, C. Schmaus, H. Spence. 2019. *Powering the Blue Economy; Exploring Opportunities for Marine Renewable Energy in Maritime Markets*. U.S. Department of Energy, Office of Energy Efficiency and Renewable Energy. Washington, D.C.

[3] OES Annual Report 2022, The Executive Committee of IEA Ocean Energy Systems. Available online: https://www.ocean-energy-systems.org/publications/oes-annual-reports/document/oes-annual-report-2022 (accessed on April 30, 2023).

[4] J. Langer, J. Quist, and K. Blok, "Recent progress in the economics of ocean thermal energy conversion: Critical review and research agenda," *Renewable and Sustainable Energy Reviews*, vol. 130, September 2020, pp. 1-11.

[5] https://www.nrel.gov/docs/fy16osti/66794.pdf

[6] S. J. Kim, and W. Koo, "Numerical Study on a Multibuoy-Type Wave Energy Converter With Hydraulic PTO System Under Real Sea Conditions," *IEEE Journal of Oceanic Engineering*, vol. 46, no.2, April 2021. pp. 573–582.

[7] L. Hai, O. Svensson, J. Isberg, and M. Leijon, "Modelling a point absorbing wave energy converter by the equivalent electric circuit theory: A feasibility study," *Journal of Applied Physics*, vol. 117, 164901, 2015.

[8] https://www.carlsbaddesal.com/

[9] H.-J. Knaak, “Modular Multilevel Converters and HVDC/FACTS: a success story”, 14th European Conference on Power Electronics and Applications (EPE), 2011.

[10] A. Lesnicar and R. Marquardt, “An innovative modular multilevel converter topology suitable for a wide power range,” in Proc. IEEE Power Tech Conf., 2003, pp. 1–6

[11] H. Nademi, "Chapter 17 - Modular Multilevel Converter (MMC) and Its Control," in *Control of Power Electronic Converters and Systems*, F. Blaabjerg Ed.: Academic Press, 2018, pp. 141-166.

[12] M. Perez, S. Bernet, J. Rodriguez, S. Kouro, and R. Lizana, "Circuit Topologies, Modeling, Control Schemes, and Applications of Modular Multilevel Converters,", *IEEE Transactions on Power Electronics,* vol. 30, no. 1, pp. 4-17, January 2015.

[13] Arizona Department of Water Resources; https://new.azwater.gov/news/articles/2022-21-01

[14] J. Prendergast, M. Li, and W. Sheng, B.G. Lee, "A Study of the Effects of Wave Spectra on Wave Energy Conversions," *IEEE Journal of Oceanic Engineering*, vol. 45, no.1, January 2020. pp. 271–283.

Appendix:

The poster was presented in the 5th Annual NSPIRE Symposium in August 2023 while presenting a poster for the design concept. The NSPIRE Symposium is a unique venue for students and faculty members in San Diego County from Scripps Research, MiraCosta community college, Palomar college, and California State University-San Marcos campuses to discuss research ideas and foster new professional relationships. In addition, CSUSM is one of the partners of the D-Enterprise (Diversifying and Engaging the Navy Through Technical Education and Recruitment Partnerships for Research Innovations in Science and Engineering) which is a program supports by the *Office of Naval Research* via Scripps Institution of Oceanography. Our marine team Captain, Miguel Lopez attended the show case event was held in August 2023 as a D-ENTERPRISE Summer Program student. This event aimed for engaging undergraduate students in research and curriculum development by assigning marine-oriented projects.

Team Captain, Miguel Lopez attended the show case event was held in August 2023 as a D-ENTERPRISE Summer Program student.

Marine team members are preparing a 3D mock-up prototype for water testing. (From right to left: Thomas Handzel, Miguel Lopez, Fares Alhabardi, and Alin Hanna)

The California State University Council on Ocean Affairs, Science and Technology (COAST) supports marine and coastal related activities within the California State University campuses. CSUSM team member, Alin Hanna, senior Electrical Engineering student and Haley Lorenz, senior student in Mathematics awarded an Undergraduate Student Research Fund for Spring semester 2024.

Marine Team hosted visitors from San Diego North County High-school Girls students as part of STEM IDEA Academy on CSUSM Campus in Fall 2023.